

# **Cumulative Millisecond-Long Sampling for a Comprehensive Energetic Evaluation of Aqueous Ionic Liquid Effects on Amino Acid Interactions**

Till El Harrar<sup>1,2</sup>, Holger Gohlke<sup>2,3,\*</sup>

<sup>1</sup> Institute of Biotechnology, RWTH Aachen University, 52074 Aachen

<sup>2</sup> John-von-Neumann-Institute for Computing (NIC), Jülich Supercomputing Centre (JSC), Institute of Biological Information Processing (IBI-7: Structural Biochemistry), and Institute of Bio- and Geosciences (IBG-4: Bioinformatics), Forschungszentrum Jülich GmbH, 52428 Jülich

<sup>3</sup> Institute for Pharmaceutical and Medicinal Chemistry, Heinrich Heine University Düsseldorf, 40225 Düsseldorf

Running title: PMF computations of pairwise amino acid interactions in aLL

\*Corresponding author:

Prof. Dr. Holger Gohlke

John-von-Neumann-Institute for Computing (NIC), Jülich Supercomputing Centre (JSC), Institute of Biological Information Processing (IBI-7: Structural Biochemistry), and Institute of Bio- and Geosciences (IBG-4: Bioinformatics)

Forschungszentrum Jülich GmbH

Wilhelm-Johnen-Str.

52428 Jülich

Email: [h.gohlke@fz-juelich.de](mailto:h.gohlke@fz-juelich.de)

# 1 Abstract

The interactions of amino acid side-chains confer diverse energetic contributions and physical properties to a protein's stability and function. Various computational tools estimate the effect of changing a given amino acid on the protein's stability based on parametrized (free) energy functions. When parametrized for the prediction of protein stability in water, such energy functions can lead to suboptimal results for other solvents, such as ionic liquids (IL), aqueous ionic liquids (aIL), or salt solutions. However, to our knowledge, no comprehensive data is available describing the energetic effect of aIL on intramolecular protein interactions. Here, we present the most comprehensive set of potential of mean force (PMF) profiles of pairwise protein-residue interactions to date, covering 50 relevant interactions in water, the two biotechnologically relevant aIL [BMIM/Cl] and [BMIM/TfO], and [Na/Cl]. These results are based on a cumulated simulation time of  $> 1$  ms. aIL and salt ions can weaken, but also strengthen, specific residue interactions by more than  $3 \text{ kcal mol}^{-1}$ , depending on the residue pair, residue-residue configuration, participating ions, and concentration, necessitating considering such interactions specifically. These changes originate from a complex interplay of competitive or cooperative noncovalent ion-residue interactions, changes in solvent structural dynamics, or unspecific charge screening effects and occur at the contact distance but also at larger, solvent-separated distances. This data provides explanations at the atomistic and energetic level for complex IL effects on protein stability and should help improve the prediction accuracy of computational tools that estimate protein stability based on (free) energy functions.

## 2 Introduction

Most proteins in nature are built with only twenty different amino acids, characterized by a unique structural motif in their side-chains<sup>1</sup>. The interactions of these side-chains confer diverse, energetic contributions and physical properties to a protein's stability and function. Computational tools, such as the Constraint Network Analysis<sup>2</sup> (CNA), FoldX<sup>3</sup>, or Rosetta<sup>4</sup>, estimate the protein stability based on (free) energy functions parametrized with respect to such energetic contributions. These tools are often used to predict the viability of substitutions for rational mutagenesis approaches<sup>5-11</sup>. In our recent work<sup>11</sup>, we investigated if changes in the unfolding free energy predicted by FoldX or structural weak spots predicted by CNA and changes in ionic liquid resistance of *Bacillus subtilis* Lipase A determined for a complete site-saturation mutagenesis library<sup>12</sup> are related. Surprisingly, we obtained low improvements in the prediction precision of favorable substitutions for FoldX compared to random mutagenesis, whereas predictions based on experimental thermostability data from CNA resulted in markedly higher improvements<sup>11</sup>. One of the reasons for the subpar results may be that the FoldX (free) energy function has been trained on data for the thermodynamic stability of proteins in water<sup>13</sup>. Hence, the function does not consider effects on interactions between protein residues by solvents other than water, e.g., organic solvents or ionic liquids.

Ionic liquids (IL) are interesting solvents and co-solvents for biotechnological approaches; when used as a co-solvent, the solutions are termed aqueous ionic liquids (aIL). At the same time, however, aIL often reduce enzyme activity<sup>12, 14-19</sup>. Many effects of IL ion-protein interactions were reported, including protein stabilization<sup>20-25</sup> and destabilization<sup>25-28</sup> on the local and global protein structure level, increased<sup>22, 29</sup> or decreased<sup>12, 18, 29-31</sup> catalytic activity, or augmented protein refolding<sup>24, 32, 33</sup> or unfolding<sup>32</sup>. The results varied depending on concentration, solvent, and enzyme, indicating that aIL show ion- and concentration-dependent effects on specific intramolecular protein interactions<sup>25, 26, 29, 32, 34</sup>. In particular, IL ions were shown to influence  $\pi$ - $\pi$ -stacking interactions<sup>35</sup>, salt bridges<sup>36</sup>, and cation- $\pi$  interactions<sup>37, 38</sup>. Our recent work showed that IL ions redistribute local enzyme stability via long-range perturbation pathways induced by specific interactions of IL ions with specific residues on the enzyme surface<sup>34</sup>. This observation is supported by NMR- and molecular dynamics (MD) simulation studies highlighting local and site-specific effects on interactions that subsequently affected the protein stability<sup>39-41</sup>. However, to our knowledge, no comprehensive data is available to predict the energetic effect of aIL on intramolecular protein interactions, which is in stark contrast to such data for intramolecular protein interactions in vacuum<sup>42-45</sup>, water<sup>42, 44-52</sup>, or other solvents, including salt solutions<sup>53</sup> and organic solvents<sup>42</sup> or based on double mutation cycle studies<sup>54</sup>. Such data, therefore, could improve the prediction precision of computational tools for estimating protein stability in aIL.

In this work, we performed extensive umbrella sampling (US) simulations of in total > 1 ms length on 50 relevant pairwise protein-residue interactions. As a result, we present the, by far, most comprehensive dataset of potential of mean force (PMF) profiles for these interactions at two concentrations in two different aIL; for comparison, we also report PMF profiles for the interactions in water and sodium chloride at two

concentrations. We show that aIL can weaken or strengthen specific residue interactions via solvent bridge-like effects, depending on the residue pair, residue conformation, participating ions, and concentration, providing an explanation at the atomistic and energetic level for complex IL ion effects on protein stability.

## 3 Results

### 3.1 Overview of modeled representative residue-residue interactions

Proteins consist of 20 proteinogenic amino acids that – depending on their sequence – determine their three-dimensional structure and, thus, their function<sup>55,56</sup>. The pairwise interaction space of all amino acids comprises 200 interactions, not yet counting that amino acids may interact in different orientations. To capture specific aIL effects on interactions that might occur on longer timescales<sup>34</sup>, we employ total simulation times of up to 3  $\mu$ s per interaction for each of the seven solvents ([BMIM/TfO], [BMIM/Cl], and [Na/Cl] at concentrations of 0, 0.2 M, and 2 M each as well as water) with 16 replicas each with a simulation time of 10 ns per replica, resulting in more than 21  $\mu$ s of sampling time for each interaction. To keep the computational burden tractable, we classified the amino acids into distinct groups according to physicochemical or structural properties and chose interactions between representative residues of each class, as done before<sup>46, 53</sup>. Depending on the interaction, we simulated the amino acids restrained to specific orientations ("linear", "stacked", and "perpendicular", and a 90° rotated T-stacked conformation described before<sup>57-61</sup>, termed "twisted"). Selected interactions were additionally simulated in different conformations or protonation states to investigate specific effects in more detail, e.g., multiple  $\pi$ - $\pi$ - and cation- $\pi$ -stacking interactions. In total, we computed PMFs of 50 residue-residue interactions (**Table 1**), requiring >1 ms of equilibration and US simulation time. The standard error of the mean was  $\leq 0.25$  kcal mol<sup>-1</sup> for 348 of 350 individual solvent PMFs when excluding the areas of a steep increase due to steric clashes at very low interaction distances. The standard error of the mean in water was  $< 0.15$  kcal mol<sup>-1</sup> for all PMFs, indicating that the higher standard error of the mean originates from the effects of ionic liquid and salt solutions (see also **Figure S1** and **Text S1** in the SI).

**Table 1: Free energies at the contact distance of interactions <sup>[a]</sup>**

Fig.	AA1	AA2	Orient.	PMF <sub>Water</sub> <sup>[b]</sup>	$\Delta G_{\text{Ref}}$ <sup>[c]</sup>	PMF <sub>IL1</sub> <sup>[b]</sup>	PMF <sub>IL2</sub> <sup>[b]</sup>	PMF <sub>NaCl</sub> <sup>[b]</sup>	$D_{\text{Water}}$ <sup>[d]</sup>	References <sup>[e]</sup>
1	Glu <sup>-</sup>	Arg <sup>+</sup>	Linear	-4.0 (-0.6)	-8.6 ± 5.0	-5.1 (-0.8)	-4.5 (-0.6)	-3.5 (+0.0)	2.8	45, 58, 62-71
S2	Glu <sup>-</sup>	Lys <sup>+</sup>	Linear	-1.5 (-0.4)	-4.0 ± 2.4	-1.8 (-0.5)	-2.2 (-0.6)	-1.1 (+0.2)	2.7	45, 58, 65, 66, 68, 70, 72-74
S3	Asp <sup>-</sup>	Arg <sup>+</sup>	Linear	-3.9 (-0.5)	-8.2 ± 5.6	-4.5 (-0.7)	-4.5 (-0.7)	-3.7 (-0.2)	2.8	45, 52, 58, 63, 64, 66-68, 70, 71
S4	Asp <sup>-</sup>	Lys <sup>+</sup>	Linear	-1.3 (-0.3)	-3.7 ± 2.4	-2.0 (-0.2)	-2.2 (-0.5)	-1.1 (+0.1)	2.7	45, 52, 58, 66, 68, 70, 72-74
S5	Gln	Gln	Linear	-1.9 (+0.3)	-1.6 ± 1.1	-2.6 (+0.3)	-2.4 (+0.4)	-1.3 (+0.3)	2.9	45, 58, 75
S7	Glu <sup>-</sup>	Glu <sup>-</sup>	Linear	+0.8 (+0.7)	-0.1 ± 0.8	+0.2 (+0.5)	-0.0 (+0.4)	-0.2 (-0.0)	4.4	58, 65, 71, 76
S8	Arg <sup>+</sup>	Arg <sup>+</sup>	Linear	+0.9 (n/a)	-0.2 ± 0.5	+0.9 (n/a)	+0.4 (-0.0)	+0.9 (n/a)	5.5	58, 65, 76
S9	Arg <sup>+</sup>	Arg <sup>+</sup>	Perpend.	+1.7 (-0.3)	-1.3 ± 0.9	-1.4 (-0.4)	-1.5 (-0.2)	-1.1 (-0.6)	4.2	58, 65, 77, 78
S10	His <sup>+</sup>	His <sup>+</sup>	Stacked	-2.6 (-0.8)	-1.5 ± 2.0	-2.9 (-0.6)	-2.3 (-0.7)	-3.1 (-1.0)	3.6	58, 65
2	Phe	Phe	Stacked	-3.0 (-0.7)	-1.9 ± 1.1	-1.4 (-2.1)	-2.0 (-2.3)	-3.0 (-0.8)	3.5	58, 79-91
S11	Phe	Tyr	Stacked	-3.6 (-1.0)	-6.0 ± 1.1*	-2.2 (-2.6)	-1.7 (-2.4)	-4.4 (-1.3)	3.6	79, 92
S12	Phe	Trp	Stacked	-3.5 (-1.0)	-2.5 ± 2.0	-2.8 (-2.8)	-3.0 (-2.4)	-4.2 (-0.9)	3.5	79, 93-97
S13	Phe	Hie	Stacked	-2.9 (-0.8)	-1.2	-0.7 (-1.7)	-2.2 (-1.8)	-2.3 (-1.0)	3.6	75
S15	Tyr	Tyr	Stacked	-4.5 (-0.9)	-1.8	-2.4 (-1.8)	-4.5 (-2.6)	-4.9 (-0.7)	3.5	75
S16	Trp	Trp	Stacked	-2.6 (-0.4)	n/a	+0.3 (-3.2)	+1.0 (-2.8)	-2.2 (-0.6)	3.6	n/a
S21	Phe	Phe	Twisted	-3.9 (-0.4)	-2.5 ± 0.8	-3.4 (-0.0)	-2.8 (-0.3)	-4.2 (-0.5)	4.9	89, 98-102
S22	Phe	Hie	Twisted	-1.2 (-0.2)	-5.1 ± 0.5*	+1.1 (-0.5)	+1.5 (-0.3)	-2.3 (-0.6)	4.5	94, 103, 104; considered equal to perp. orientation
S23	Phe	Phe	Perpend.	-3.1 (-0.7)	-2.5 ± 0.5	-2.5 (-0.4)	-2.3 (-0.4)	-2.9 (-0.5)	5.0	80, 85-91, 98, 105, 106
2	Hie	Hie	Stacked	-2.6 (-0.6)	-4.6 ± 2.5*	-2.5 (-1.4)	-2.5 (-1.2)	-3.0 (-0.7)	3.6	75, 94
S18	Hid	Hid	Stacked	-2.8 (-0.9)	-4.6 ± 2.5*	-2.3 (-1.6)	-0.7 (-1.5)	-3.7 (-1.3)	3.5	75, 94
S19	Hie	Hid	Stacked	-3.7 (-0.9)	-4.6 ± 2.5*	-2.4 (-1.1)	-2.8 (-1.2)	-2.9 (-0.3)	3.5	75, 94
S20	Hie	His <sup>+</sup>	Stacked	-3.9 (-0.9)	n/a	-3.9 (-0.6)	-2.8 (-0.4)	-3.7 (-0.9)	3.5	n/a
3	Phe	Arg <sup>+</sup>	Stacked	-3.2 (-0.4)	-3.2	-3.0 (-0.4)	-2.9 (+0.1)	-4.5 (-0.9)	3.7	107
3	Arg <sup>+</sup>	Arg <sup>+</sup>	Stacked	-2.4 (-0.3)	-3.2 ± 4.0	-2.4 (-0.1)	-2.0 (-0.3)	-3.2 (-0.5)	3.6	58, 61, 65, 76-78, 108-113
S38	Phe	Leu	Perpend.	-1.8 (-0.7)	-1.3 ± 0.6	-1.3 (-0.8)	-1.7 (-0.6)	-2.0 (-0.7)	3.9	73, 86, 97, 105, 114-117; reference data for Phe-Ala shown
S24	Ala	Ala	Linear	-0.2 (-0.1)	-0.7 ± 0.3	-0.4 (-0.1)	-0.3 (-0.0)	-0.6 (-0.2)	3.7	82, 86, 118
S27	Leu	Leu	Linear	-0.0 (+0.2)	-1.2 ± 0.3	-0.0 (+0.3)	-0.1 (+0.3)	-0.2 (+0.1)	4.2	67, 82
S34	Phe	Met	Stacked	-1.3 (-0.1)	-1.4	-1.3 (-0.7)	-1.2 (-0.4)	-1.8 (-0.3)	4.0	75; reference data for Tyr-Met shown
S14	Phe	His <sup>+</sup>	Stacked	-4.8 (-1.0)	n/a	-2.9 (-0.5)	-3.5 (-0.2)	-5.9 (-1.2)	3.5	n/a

<sup>[a]</sup> Amino acids are colored according to their class: charged (red), aromatic (magenta), aliphatic (blue), and polar (orange). The overview is limited to interactions discussed in more detail in this manuscript and interactions showing the most pronounced changes.

<sup>[b]</sup> Free energies at the contact distances for interactions in water, 2 M [BMIM/Cl] (IL1), 2 M [BMIM/TfO] (IL2), and 2 M [Na/Cl]. Values in brackets denote the free energies at the solvent-separated interaction distance if existing. All individual PMF profiles were anchored to a value of 0 kcal mol<sup>-1</sup> at the final separation distance of 12.0 Å, i.e., the completely unbound state. Values are shown in kcal mol<sup>-1</sup>.

<sup>[c]</sup> Mean ± standard deviation of free energies at the contact distance or interaction minima reported in other studies investigating identical or very similar systems, e.g., side chain or functional group analogs of amino acids. Values are shown in kcal mol<sup>-1</sup>. Data reported for similar side-chain analogs or functional group analogs was considered for both residues, e.g., acetate and propionic acid for Glu<sup>-</sup> and Asp<sup>-</sup>. No distinction was made

between the data reported for N $\epsilon$ - and N $\delta$ -protonated histidines. Data from gas-phase experiments were excluded for interactions involving charged and polar residues in favor of data in solution, if possible (otherwise indicated by an asterisk), as the lack of desolvation penalty often results in substantially stronger interactions. Interactions where adequate reference studies were not available are indicated via n/a.

<sup>[d]</sup> Contact distances observed in our PMFs for the interactions in water. Values are shown in Å.

<sup>[e]</sup> References for <sup>[c]</sup>.

### 3.2 aIL stabilize both like- and opposite-charged interactions as opposed to only like-charged interactions in salt solutions

First, we investigated the behavior of charged interactions in aIL, as the interactions of opposite-charged residues (salt bridges), such as acidic residues ( $\text{Glu}^-$ ,  $\text{Asp}^-$ ) with alkaline residues ( $\text{Lys}^+$ ,  $\text{Arg}^+$ ,  $\text{His}^+$ ), are the strongest noncovalent pairwise residue interactions in proteins<sup>45, 49</sup>. Charged residues are predominantly located at the exposed protein surface and, therefore, are highly susceptible to interactions with solvent molecules, such as water or ions<sup>119</sup>. Due to the ionic composition of aIL, it is particularly interesting to identify effects originating from, e.g., competition of aIL ions with interaction partners in protein salt bridges or like-charged residue pairs as previously described for other ionic solvent species<sup>120, 121</sup>.

As a representative interaction of salt bridges, we investigated the linear  $\text{Glu}^-$ - $\text{Arg}^+$  interaction (**Figure 1**), which is the strongest salt bridge in proteins<sup>45, 49</sup>. Furthermore, the longer side-chains of  $\text{Glu}^-$  and  $\text{Arg}^+$  compared to  $\text{Asp}^-$  and  $\text{Lys}^+$ , respectively, reduce a potential impact caused by solvation effects of the backbone structure<sup>122-125</sup>. We used the distance of the center-of-mass of the  $\text{O}_\epsilon$  atoms of  $\text{Glu}^-$  and the center-of-mass of both  $\text{N}_\eta$  atoms of  $\text{Arg}^+$  as the reaction coordinate.

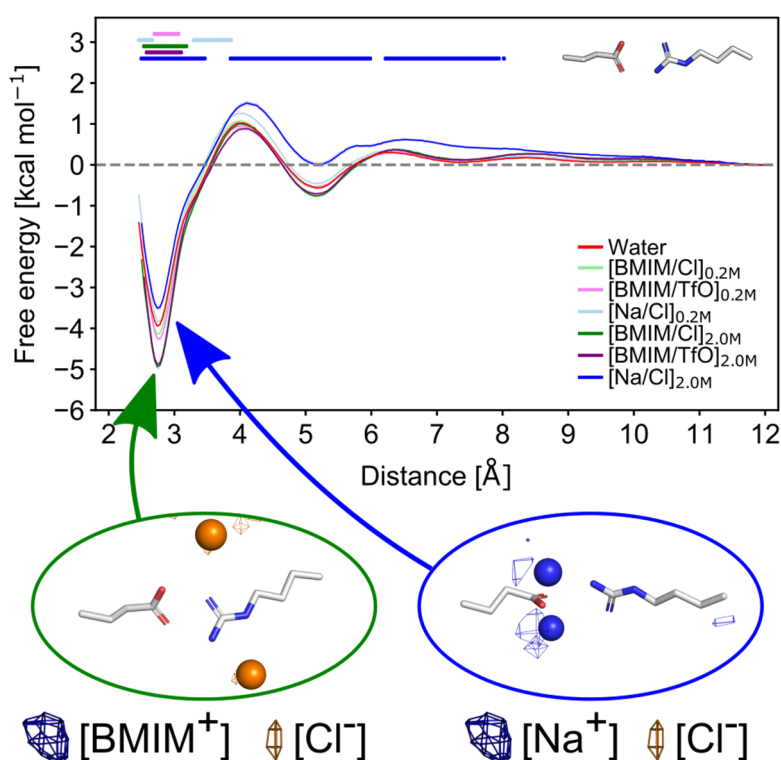


**Figure 1: PMFs of the linear interaction of  $\text{Glu}^-$ - $\text{Arg}^+$ .** PMFs in water (red), aIL ([BMIM/Cl] (0.2 M: light green; 2 M: green), [BMIM/TfO] (0.2 M: pink; 2 M: purple)), and [Na/Cl] (0.2 M: light blue and 2 M: blue). Data is shown as mean  $\pm$  standard error of the mean. Relevant ( $> 0.25 \text{ kcal mol}^{-1}$ ) and significant ( $p < 0.05$ ; determined via independent Student's  $t$ -test) differences of aIL with respect to water are indicated via colored dots above the PMFs in the respective color. For both interactions, average densities of windows showing representative states (indicated by arrows) are shown for cations (blue meshes) and anions (orange meshes) for 2 M [BMIM/Cl], 2 M [BMIM/TfO], and 2 M [Na/Cl], respectively. All distributions were normalized according to the number of frames.  $\sigma$ -values defining the intensity cutoff of the represented data of 0.05 for



[BMIM<sup>+</sup>] and [TfO<sup>-</sup>] ions and 0.005 for [Na<sup>+</sup>] and [Cl<sup>-</sup>] were used. Atoms of the capping groups and backbone atoms (N, C, O) in the residue structures are omitted for clarity.

In water, the global minimum representing the contact distance (CD) was located at a distance of 2.8 Å with -4.0 kcal mol<sup>-1</sup>, adjacent to the global maximum at 4.1 Å with a height of 1.1 kcal mol<sup>-1</sup>, suggesting disfavorable desolvation processes upon binding. With increasing distance, additional and more shallow local minima and maxima located at 5.2 Å (-0.6 kcal mol<sup>-1</sup>) and 6.3 Å (0.4 kcal mol<sup>-1</sup>), respectively, were encountered, representing the solvent-separated minimum (SSM) and a second unbeneficial energetic barrier. The PMF profiles partly agree with previous results obtained from geometry-optimized structures or *ab initio* calculations of amino acid analogs, which yielded contact distances of 2.7-3.0 Å in an aqueous environment<sup>45, 126, 127</sup>, albeit higher interaction energies of up to -17.5 kcal mol<sup>-1</sup> were predicted. Note, though, that QM computations often do not consider changes in the interaction energies caused by, for instance, configurational entropy or water solvation effects, which usually dramatically reduce the interaction energies<sup>45</sup>. In contrast, our PMFs here and in the following chapters consider these effects. Furthermore, our results consolidate findings from previous MD simulations (see **Table 1** for an overview of reference data) almost exclusively based on side-chain and functional group analogs in water, which mostly showed CDs of 2.6-3.0 Å with a free energy minimum of  $-8.6 \pm 5.0$  kcal mol<sup>-1</sup> and SSMs around 5 Å, respectively<sup>52, 58, 62-65, 128-131</sup>.

The PMFs of this interaction in aIL and salt solutions differ in part significantly. E.g., the interaction was destabilized in 2 M [Na/Cl] by ~0.5 kcal mol<sup>-1</sup> at lower distances up to the first SSM, likely mediated by charge screening effects of [Na<sup>+</sup>] following the Debye-Hückel theory<sup>132</sup>, according to which the free energy of salt bridges is lower with increasing ionic strength, as well as interactions of [Na<sup>+</sup>] with Glu<sup>-</sup>, competing with Arg<sup>+</sup>. Similar observations in previous studies support our findings (see **Text S2** in the SI for detailed information). In contrast, aIL stabilized the interaction around the CD by up to 1.1 kcal mol<sup>-1</sup> in 2 M [BMIM/Cl] and 2 M [BMIM/TfO], which is counterintuitive at first as to the Debye-Hückel theory<sup>132</sup>. However, compared to [Na<sup>+</sup>], [BMIM<sup>+</sup>] ions are too voluminous to arrange between the Glu<sup>-</sup>-Arg<sup>+</sup> residue pair at short distances and, thus, do not show the destabilizing behavior of [Na/Cl] solutions. Instead, [Cl<sup>-</sup>] or ions accumulate at the N<sub>ε</sub> atom of Arg<sup>+</sup> in [BMIM/Cl], potentially inducing a water structure-breaking effect<sup>133</sup> and leading to the observed stabilization effect due to a reduced desolvation penalty upon salt bridge association.

Other salt bridges involving opposite-charged residue pairs of Glu<sup>-</sup> and Asp<sup>-</sup> with Arg<sup>+</sup> and Lys<sup>+</sup> (see **Figures S2-S4** in the SI) resulted in similar-shaped PMF profiles, showing the destabilizing and stabilizing effects of salt solutions and aIL, respectively. The same effect was also observed for the strong polar interaction of two glutamine residues (see **Figure S5**) but not for the weak polar interaction of a serine pair (see **Figure S6**), indicating that interaction-specific differences in the induced effect of aIL incubation exist. Surprisingly, we also observed solvent-specific stabilization effects of aIL for like-charged residue pairs of Glu<sup>-</sup>, Arg<sup>+</sup>, or His<sup>+</sup>, which are common structural motifs in proteins despite their intuitively repelling nature<sup>61</sup>,

<sup>134-137</sup> (**Figures S7-S10** and **Text S3** in the SI). For instance, the linear Glu<sup>-</sup>-Glu<sup>-</sup> interaction (**Figure S7**) was stabilized by  $\sim 0.8$  kcal mol<sup>-1</sup> in high concentrations of aIL compared to water, resulting in a novel stable interaction minima of 0 kcal mol<sup>-1</sup> at 4.4 Å. This effect was described previously for ethylenediaminetetraacetic acid (EDTA) aggregates and similar structural arrangements in salt solutions, such as [Na/Cl], where [Na<sup>+</sup>] ions coordinated between the two bilayers of carboxylic acid moieties of EDTA molecules, stabilizing the arrangement via direct electrostatic interactions and charge screening effects<sup>138-141</sup>. In contrast, ion density analyses (**Figure S7**) indicate that IL ions are too bulky to coordinate between the residue pair and likely stabilize the interaction via charge screening effects, agreeing with the lower degree of stabilization. On the other hand, we observed ion-specific effects of [TfO<sup>-</sup>] ions on positively charged residue pairs of Arg<sup>+</sup> and His<sup>+</sup> around the SSM (**Figures S8-S10**), where ion density analyses indicate that [TfO<sup>-</sup>] ions stabilize the interaction via direct interactions and charge screening effects similar to [Na<sup>+</sup>] between EDTA molecules.

To conclude, our results indicate solvent bridge-like effects of aIL ions on opposite- and like-charged interactions. As a result, aIL ions stabilize both like- and opposite-charged intramolecular protein residue interactions. In contrast, inorganic salt ions stabilized only like-charged interactions, whereas opposite-charged interactions, e.g., salt bridges, were destabilized.

### 3.3 aIL ions modify $\pi$ -stacking interaction characteristics via stabilizing and destabilizing effects

Next, we analyzed planar  $\pi$ -stacking interactions of aromatic amino acids, such as Phe, Trp, His, and Tyr, as they play vital roles in molecular recognition processes<sup>142-146</sup> or folding and structural stability of proteins<sup>147-150</sup> (**Figure 2** and **Figures S10-S20**). Furthermore, experimental and computational studies revealed a perturbation of solvent-exposed  $\pi$ -stacking interactions in proteins by [BMIM<sup>+</sup>] ions<sup>34,35</sup>. For all interactions, we used the distance of the center-of-mass of the aromatic moieties as a reaction coordinate.

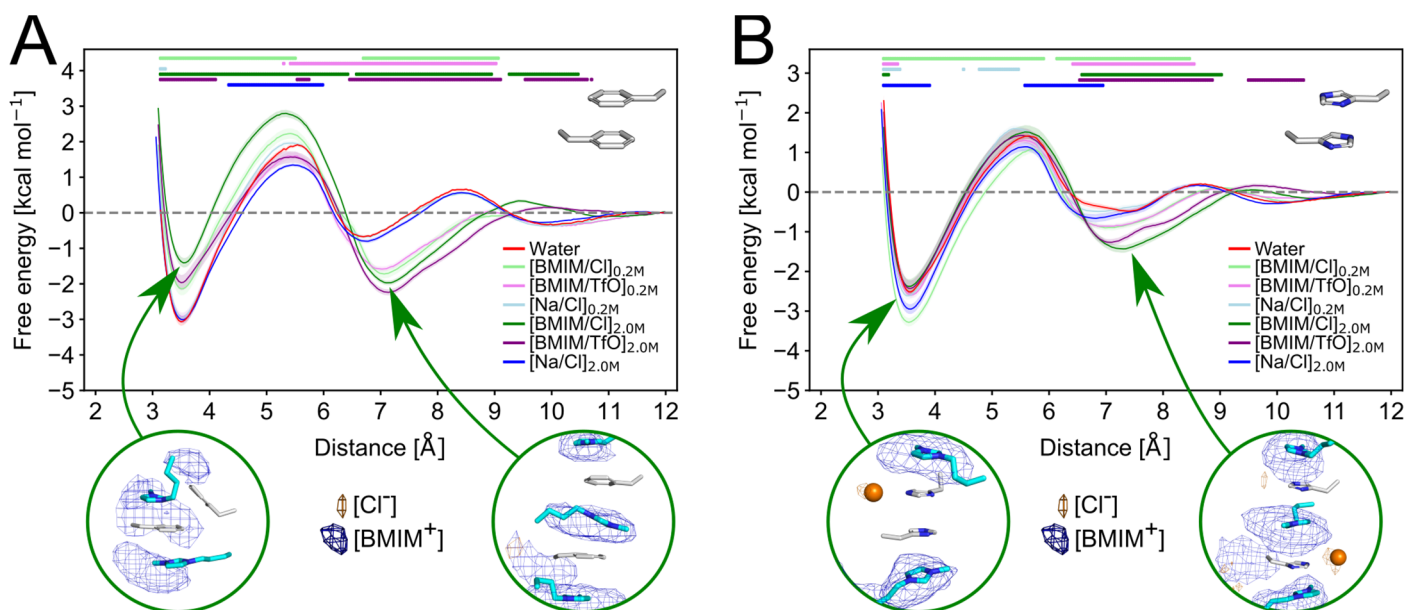


**Figure 2: Differences in the perturbation tolerance between  $\pi$ -stacking interactions, pointing to a novel substitution pattern for rational mutagenesis approaches.** A-B: PMFs of planar Phe-Phe (A) and planar His-His (B) in water (red), aIL ([BMIM/Cl] (0.2 M: light green; 2 M: green), [BMIM/TfO] (0.2 M: pink; 2 M: purple)), and [Na/Cl] (0.2 M: light blue and 2 M: blue). Data is shown as mean  $\pm$  standard error of the mean. Relevant ( $> 0.25$  kcal mol<sup>-1</sup>) and significant ( $p < 0.05$ ; determined via independent Student's  $t$ -test) differences of aIL with respect to water are indicated via colored dots above the PMFs in the respective color. For both interactions, average densities of windows showing representative states (indicated by arrows) are shown for cations (blue meshes) and anions (orange meshes) for 2 M [BMIM/Cl], 2 M [BMIM/TfO], and 0.2 M or 2 M [Na/Cl], respectively. All distributions were normalized according to the number of frames.  $\sigma$ -values defining the intensity cutoff of the represented data of 0.05 for [BMIM<sup>+</sup>] and [TfO<sup>-</sup>] ions, and 0.005 for [Na<sup>+</sup>] and [Cl<sup>-</sup>], were used. Atoms of the capping groups and backbone atoms (N, C, O) in the residue structures are omitted for clarity.

First, we investigated the planar  $\pi$ -stacked Phe-Phe interaction (**Figure 2A**), as Phe is the most frequently occurring aromatic amino acid in proteins<sup>151-154</sup>. Additionally, it comprises the least complex structural motif of all aromatic amino acids and is frequently investigated in QM and experimental studies as a prototype for more complex  $\pi$ -systems<sup>98, 135, 155-158</sup>.

The global minimum representing the CD was located at 3.5 Å with  $-3.0 \text{ kcal mol}^{-1}$ . An energy barrier of  $1.8 \text{ kcal mol}^{-1}$  at 5.7 Å separated it from a stable SSM located at 6.6 Å with a depth of  $-0.7 \text{ kcal mol}^{-1}$ , again indicating energetically unbeneficial desolvation processes upon binding. With further increasing distance, a second SSM with  $-0.5 \text{ kcal mol}^{-1}$  at 10.0 Å was encountered, separated by an additional local maximum at 8.5 Å of  $0.7 \text{ kcal mol}^{-1}$ . The locations of interaction minima and maxima agree with previously computed PMFs of benzene and toluene dimers in water using MD simulations, albeit higher-level theory QM studies<sup>83, 87-89, 118</sup> predict slightly higher contact distances of 3.8-3.9 Å with slightly lower interaction and binding energies from  $-1.02$  to  $-1.88 \text{ kcal mol}^{-1}$  (see **Text S4** in the SI).

Incubation in aIL and salt solutions led to significant changes in the PMFs of this interaction. 2.0 M aIL substantially destabilized the interaction at the CD by up to  $1.6 \text{ kcal mol}^{-1}$  while stabilizing the SSM by up to  $1.6 \text{ kcal mol}^{-1}$ , making the SSM the energetically most favorable state. The SSM additionally shifted by 0.5 Å to higher distances. Around the CD, [BMIM<sup>+</sup>] ions accumulate next to the interface formed by the aromatic moieties of the amino acids, competing for  $\pi$ -stacking/ $\pi$ -cation and hydrophobic interactions and effectively pushing the residues apart (**Figure 2A**). In this regard, quantum-mechanically geometry-optimized trimers of benzene arranged in a pinwheel-like structure as the preferred orientation support the hypothesis that additional molecules containing  $\pi$ -systems can disrupt an existing  $\pi$ -stacking dimeric interaction<sup>150, 159</sup>. In contrast to destabilizing effects at the CD, [BMIM<sup>+</sup>] ions act as solvent bridge-like molecules at the SSM, forming face-to-face  $\pi$ -stacking/ $\pi$ -cation residue-ion-residue clusters (**Figure 2A**), similar to stabilizing effects of [Na<sup>+</sup>], [BMIM<sup>+</sup>], and [TfO<sup>-</sup>] in like-charged interactions of residue pairs of Glu<sup>-</sup>, Arg<sup>+</sup>, or His<sup>+</sup> (**Figure 3, Figures S7-S10**). Increased densities at the top and the bottom of this arrangement indicate that two additional ion layers form, as observed for other  $\pi$ -stacking/ $\pi$ -cation systems<sup>134, 160</sup>. These effects were not observed for the salt solutions and only weakly for 0.2 M aIL, indicating a [BMIM<sup>+</sup>] concentration-dependent effect on  $\pi$ -stacking interactions. Similar-shaped PMF profiles and the destabilizing and stabilizing effects of aIL at higher concentrations were observed for most other planar interactions of aromatic amino acids (see **Figures S10-S20** in the SI). Notably, the destabilizing and stabilizing effects were conformation-specific, as perpendicular or twisted interactions of aromatic amino acids were perturbed at lower distances but not stabilized around the SSM (**Figures S21-S23**; see **Text S5** in the SI).

In contrast, the interactions of aliphatic yet non-aromatic amino acid pairs, such as alanine, valine, leucine, or isoleucine residue pairs, experienced no substantial effect of aIL and salt solutions. These interactions showed only very weak ( $\leq 0.25 \text{ kcal mol}^{-1}$ ) and no consistent differences from the water simulations (**Figures S24-S28** and **Text S6** in the SI). These observations further indicate that aromaticity is a crucial residue feature determining the effects on aromatic residues upon incubation in aIL and salt solutions. Furthermore, self-solvation effects, preferential interactions of aIL and salt ions with the residue backbone, and the residue backbone desolvation upon binding might play an increasingly important role in more compact amino acids<sup>122-125</sup>. These forces might exceed the direct effects of aIL and salt solutions, as the residues interact weaker with IL ions than aromatic and charged residues<sup>34</sup>.

Interestingly,  $\pi$ -alkyl- and methionine- $\pi$ -interactions partly showed stabilizing and destabilizing effects similar to  $\pi$ - $\pi$ -interactions in aIL and salt solutions, albeit weaker, further highlighting the importance of aromaticity. For more details, see **Figures S29** and **Text S7** or **Figure S30-S31** and **Text S8** in the SI, respectively.

Next, we investigated the  $\pi$ -stacking interaction of two neutral  $N_\epsilon$ -protonated histidines (**Figure 2B**). Due to its multiple protonation states<sup>161</sup>, its ability to act as H-bond donor<sup>162</sup> or acceptor<sup>163</sup>, and the possibility to participate in  $\pi$ - $\pi$ - and cation- $\pi$ -stacking interactions<sup>51, 164</sup>, histidine is probably the most versatile of the 20 natural amino acids<sup>165</sup>. Furthermore, apart from the role in protein folding and protein stability<sup>51, 164</sup>, it is a crucial residue in many catalytic sites<sup>166-168</sup>, molecular recognition processes<sup>169</sup>, resulting in histidine dimers frequently occurring in protein structures<sup>169</sup>.

In general, the His-His interaction showed a similar-shaped PMF profile to the Phe-Phe interaction in water, with a global minimum at the CD of 3.6 Å with  $-2.6 \text{ kcal mol}^{-1}$  and a stable SSM around 7 Å with  $-0.6 \text{ kcal mol}^{-1}$ , separated by an energy barrier at 5.3 Å with a height of  $1.5 \text{ kcal mol}^{-1}$ , again indicating an energetically unbeneficial desolvation process upon binding. However, our results agree qualitatively with the PMF obtained for the parallel stacked histidine dimer investigated in ref. <sup>75</sup>, which reported slightly higher contact distances of 4.5 Å with a free energy of  $-1.1 \text{ kcal mol}^{-1}$ , and quantum-mechanically determined interaction distances of antiparallel-stacked dimers of histidine from ref. <sup>169</sup> reporting CDs from 3.4-3.6 Å<sup>169</sup>. Notably, aIL overall showed no substantial effect on the location or depth of the minimum at the CD. In contrast, 2 M [Na/Cl] slightly increased the interaction strength by  $-0.4 \text{ kcal mol}^{-1}$ . The spatial distribution analysis revealed increased anion densities close to the contact interface, likely stabilizing the residue interaction via coordination effects. Such a stabilizing coordination effect has been described for [Cl<sup>-</sup>] located at the periphery of  $\pi$ - $\pi$ -stacking interactions of imidazolium ions, mediated by H-bonds between [Cl<sup>-</sup>] and the imidazolium ions<sup>170</sup>. Furthermore, the SSM at 7.0 Å was deeper in aIL than in water, reminiscent of what was found for the Phe-Phe interaction, where [BMIM<sup>+</sup>] ions located between both residues acted as solvent bridge-like molecules by forming face-to-face  $\pi$ -stacking and  $\pi$ -cation interactions. The PMF profiles of other protonation states of histidine residue pairs are generally similar, as are the aIL-induced effects (**Figures S10** and **Figures S18-S20**). However, solvent-specific differences in the destabilization of the stacked interaction of two histidines exist, as the dimer of two  $N_\delta$ -protonated histidines was destabilized in 2 M [BMIM/TfO] but not 2 M [BMIM/Cl]. These observations indicate protonation state-specific effects, highlighting the importance of assigning the correct protonation states of titratable amino acids in MD simulations. Notably, interactions involving at least one double-protonated, positively charged His<sup>+</sup> residue also showed pronounced ion-specific effects (**Figure S10** and **Figures S20**). Previous QM studies predicted stable  $\pi^+-\pi^+$ -arrangements for host-guest systems employing this structural motif<sup>171</sup>, supporting the observed stable His<sup>+</sup>-His<sup>+</sup> interaction despite strong repulsion forces. In His<sup>0</sup>-His<sup>+</sup>, high concentrations of [BMIM/TfO] induced a similar destabilizing effect of  $\sim 1 \text{ kcal mol}^{-1}$  at distances below the SSM as observed for other aromatic amino acid pairs. The spatial distribution analysis suggests that [TfO<sup>-</sup>] ions accumulating at the contact interfaces induce

these perturbations in that they compete for noncovalent interactions, effectively pushing the residues apart. These interactions include strong electrostatic interactions with the positively charged histidine as well as H-bonds and hydrophobic tethers. 2 M [BMIM/Cl] did not show the same effect despite a similar accumulation of [Cl<sup>-</sup>] at the contact interfaces, likely due to the much weaker interactions of [Cl<sup>-</sup>] to His and His<sup>+</sup> compared to [TfO<sup>-</sup>]<sup>34</sup>. The increased interaction strength of His<sup>+</sup>-His compared to His-His is in good accordance with other studies<sup>165, 172</sup>, e.g., increased binding energies of the cationic compared to the neutral benzene dimer<sup>173</sup>.

To conclude, our results revealed system-specific solvent bridge and perturbation effects of aIL on most arrangements comprising two  $\pi$ -systems. Similar to the observations in like- and opposite-charged residue interactions, these effects were mediated by competitive or coordinative noncovalent interactions of [BMIM<sup>+</sup>] and [TfO<sup>-</sup>] ions with the residue pair. Notably, we observed residue- and conformation-specific effects for the planar  $\pi$ -stacking interaction of two residues comprising aromatic motifs, indicating that some interactions are more tolerant to aIL-induced perturbation effects than others.

### 3.4 Almost all other investigated interactions experience substantial effects in the presence of IL ions

Finally, we investigated various other interactions with crucial roles in protein folding, protein stability, or molecular recognition processes<sup>51, 61, 134-137, 174-176</sup>, including interactions involving residues from different classes, and highlight two selected interactions here: the planar  $\pi$ -cation-stacking Phe-Arg<sup>+</sup> interaction, and the planar Arg<sup>+</sup>-Arg<sup>+</sup> stacking interaction (**Figure 3** and **Figures S29-S46**).

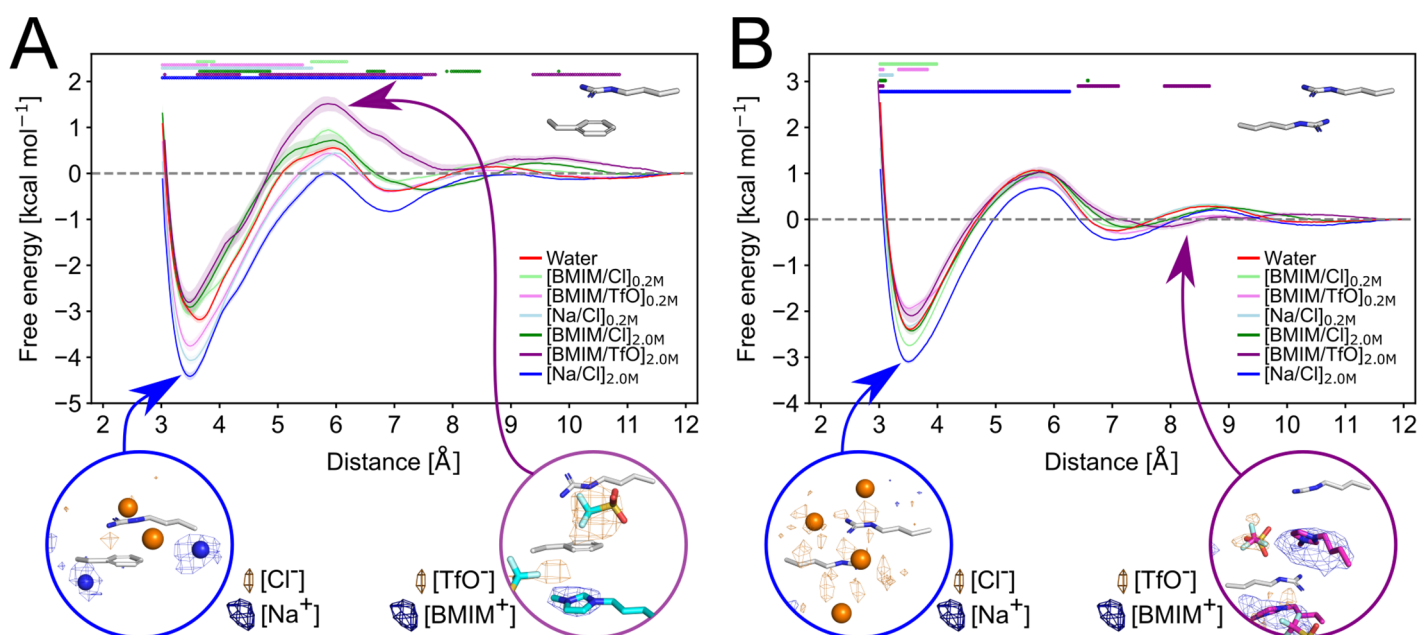


**Figure 3: PMFs of mixed residue interactions.** PMF of the planar  $\pi$ -cation Phe-Arg<sup>+</sup> interaction (A), and the stacking interaction of Arg<sup>+</sup>-Arg<sup>+</sup> (B) in water (red), aIL ([BMIM/Cl] (0.2 M: light green; 2 M: green), [BMIM/TfO] (0.2 M: pink; 2 M: purple)), and [Na/Cl] (0.2 M: light blue and 2 M: blue). Data is shown as mean  $\pm$  standard error of the mean. Relevant ( $> 0.25$  kcal mol<sup>-1</sup>) and significant ( $p < 0.05$ ; determined via independent Student's *t*-test) differences of aIL with respect to water are indicated via colored dots above the

PMFs in the respective color. For all interactions, average densities of windows showing representative states (indicated by arrows) are shown for cations (blue meshes) and anions (orange meshes). All distributions were normalized according to the number of frames.  $\sigma$ -values defining the intensity cutoff of the represented data of 0.05 for [BMIM<sup>+</sup>] and [TfO<sup>-</sup>] ions, and 0.005 for [Na<sup>+</sup>] and [Cl<sup>-</sup>], were used. Atoms of the capping groups and backbone atoms (N, C, O) in the residue structures are omitted for clarity.

First, we investigated the planar interaction of Phe-Arg<sup>+</sup> as a representative for cation- $\pi$ -interactions (**Figure 3A**). Cation- $\pi$ -interactions between aromatic (Phe, Tyr, Trp, His) and positively-charged (Arg<sup>+</sup>, Lys<sup>+</sup>, His<sup>+</sup>) amino acids are common structural motifs in protein crystal structures and essential for molecular recognition and protein stability<sup>51, 135, 174-176</sup>.

In water, the global minimum representing the CD was located at a distance of 3.7 Å with -3.2 kcal mol<sup>-1</sup>, adjacent to the global maximum at 6.0 Å with 0.5 kcal mol<sup>-1</sup>, indicating unfavorable desolvation processes upon binding. The SSM was encountered at 6.9 Å (-0.4 kcal mol<sup>-1</sup>), followed by a second energetic barrier at 8.8 Å (0.2 kcal mol<sup>-1</sup>). The results are in good agreement with QM calculations<sup>51, 177</sup> and previously performed PMF calculations<sup>46</sup> (see **Text S9** in the SI).

Incubation in 0.2 M and 2 M [Na/Cl] stabilized the interaction by ~1.0 kcal mol<sup>-1</sup>, whereas incubation in 2 M [BMIM/TfO] showed destabilizing effects of up to ~1.0 kcal mol<sup>-1</sup> around the SSM. The spatial distribution and cluster analysis indicated that the stabilization effect is due to [Na<sup>+</sup>] and [Cl<sup>-</sup>] accumulating around the contact interface and the molecule backbone, forming stabilizing ion bridge-like structures, whereas [BMIM<sup>+</sup>] and [TfO<sup>-</sup>] ions likely destabilized the interaction by forming competing interactions with Phe and Arg<sup>+</sup>, respectively. This observation is in good agreement with the observed impact of [BMIM<sup>+</sup>] or [TfO<sup>-</sup>] on other interactions comprising  $\pi$ -systems or positively charged residue pairs, respectively (**Figure S8-S23**) and preferential interactions of polar or opposite-charged solvent molecules with cationic  $\pi$ -systems leading to a displaced rather than the sandwich-stacked conformation<sup>178</sup>.

Second, we investigated the planar stacking interaction of two arginine residues (**Figure 3B**), a recurring motif often observed in protein crystal structures<sup>61, 134-137</sup>. Additionally, stable guanidinium pairs in aqueous guanidinium salt solutions, stabilized by a combination of dispersion and cavitation forces exceeding the Coulomb repulsion<sup>60</sup>, were suggested in simulations<sup>58, 60, 61, 78, 108</sup> and experiments<sup>179-181</sup>. We used the distance of the centers-of-mass of the guanidinium moieties as a reaction coordinate.

The global minimum representing the CD was located at 3.6 Å with -2.4 kcal mol<sup>-1</sup>. A high energy barrier of 0.8 kcal mol<sup>-1</sup> at 5.9 Å separated it from a stable SSM located at 7.1 Å with a depth of -0.3 kcal mol<sup>-1</sup>, again indicating energetically unbeneficial desolvation processes upon binding. An additional local maximum at 8.7 Å of 0.3 kcal mol<sup>-1</sup> was encountered with further increasing distance. Our results agree well with the preferred arginine stacking C $\zeta$ -C $\zeta$  distance of ~3.8 Å in crystal structures<sup>134, 182</sup> and QM calculations of guanidinium stacking in water<sup>78, 110, 183</sup> (see **Text S10** in the SI). Our results, therefore, extend previous MD

studies of side-chain analogs reporting vague interaction free energies of  $-3.2 \pm 4.0$  kcal mol<sup>-1</sup> at varying CDs, depending on the water model and simulation setup<sup>57-59, 180, 184</sup>.

Incubation in 2 M [Na/Cl] marginally stabilized the interaction by  $\sim 0.3$  kcal mol<sup>-1</sup> at distances below the SSM. The spatial distribution and cluster analysis indicate that [Cl<sup>-</sup>] ions accumulate around the contact interfaces, likely inducing the stabilization via electrostatic coordination and charge screening effects. Previous MD studies of 3 M [Gdm/Cl] and 1.5 M [Gdm<sub>2</sub>/SO<sub>4</sub>] solutions reported an increased separation distance of guanidinium interactions of 3.8-4.0 Å as compared to  $\sim 3.0$ -3.4 Å in water<sup>160, 185</sup>, suggested to be caused by the inclusion of counterions<sup>160, 180, 185</sup>. In contrast, QM calculations indicate that the exclusion of counterions led to a decrease in interaction strength<sup>183</sup>, in line with our predictions, similar to the coordination effects observed for [Cl<sup>-</sup>] ions on the stable association of 1,3-dimethyl imidazolium ions<sup>170</sup>. High concentrations of [BMIM/Cl] or [BMIM/TfO] led to stabilization effects at the SSM, with 2 M [BMIM/TfO] showing a slightly stronger magnitude, whereas this effect did not occur in 2 M [Na/Cl]. This corroborates ion-specific effects on distinct interactions. Analyses of ion densities indicate the existence of Arg<sup>+</sup>-[BMIM<sup>+</sup>]-Arg<sup>+</sup> clusters at high concentrations of [BMIM<sup>+</sup>] ions, stabilizing the interaction of two positively-charged  $\pi$ -systems in a similar fashion as observed for the stacked His<sup>+</sup>-His<sup>+</sup> interaction (**Figure S10**). The stronger stabilization in [BMIM/TfO] is likely mediated by charge screening effects induced by accumulation of [TfO<sup>-</sup>] ions around the Arg<sup>+</sup>-[BMIM<sup>+</sup>]-Arg<sup>+</sup> clusters.

To conclude, our results revealed system-specific solvent bridge and perturbation effects of aIL on various interactions between different residue classes mediated by strong interactions of [BMIM<sup>+</sup>] or [TfO<sup>-</sup>] ions with one or both residues. These interactions can be competitive at lower distances and stabilizing at higher distances, as observed for like-charged residue pairs or interactions comprising  $\pi$ -systems. In contrast, salt solutions mostly stabilized the interactions around the contact distances via weak coordinating effects. Further, the excellent agreement of our PMF profiles with various experimental observations of unintuitive or often overlooked structural motifs indicates a good representation of intramolecular forces by our simulations.

## 4 Discussion

In this work, we systematically computed a comprehensive set of PMF profiles for representative pairwise protein residue interactions in aIL and revealed solvent-, ion-, and concentration-specific effects. We showed that IL and salt ions can substantially destabilize but also stabilize pairwise residue interactions by up to 3.6 kcal mol<sup>-1</sup> in the planar  $\pi$ - $\pi$ -stacking interaction of Trp-Trp (**Figure S16**), potentially introducing unbeneficial structural changes in protein structures<sup>16, 30, 34, 35, 41</sup>. The effects are markedly influenced by the interaction strength of the solvent ions with both residues, the conformation-specific binding mode, and the solvent concentration. Overall, we observed the following trends:



- Ions forming strong interactions with one or both residues with interaction energies comparable or higher to that of the residue interaction destabilize the interaction around the contact distance induced by strong competitive noncovalent interactions, e.g., [BMIM<sup>+</sup>] in many  $\pi$ - $\pi$ -stacking interactions (**Figure 2**). On the other hand, the same ion often stabilizes the interaction around the SSM by acting as a solvent bridge between both residues using these strong noncovalent forces.
- Ions forming preferential interactions with both residues with interaction energies weaker than the residue interaction stabilize the interaction mediated by coordinating effects, such as preferential interactions with both residues, or nonspecific charge screening, e.g., observed for [BMIM<sup>+</sup>] or [Na<sup>+</sup>] on the like-charged interaction of two glutamates (**Figure 1**).
- Ions forming no or very weak interactions with both residues usually do not affect the interaction strength (**Figures S6/S24-S28**).

This knowledge helps to understand better the effects of aIL on the structural stability of proteins. Further, it could improve the prediction accuracy of computational tools that predict changes in protein stability in these solvents upon substitution based on the strength of intramolecular forces. Notably, in rare cases, competitive or cooperative effects from two solvent ions can result in further modifications, as observed for Arg<sup>+</sup>-[BMIM<sup>+</sup>]-Arg<sup>+</sup> clusters in 2 M [BMIM/TfO], where the accumulation of [TfO<sup>-</sup>] anions around the interaction interface further stabilized instead of weakened the structural arrangement compared to [BMIM/Cl] (**Figure 3B**).

Our results are based on extensive all-atom US simulations with a combined simulation time of 21  $\mu$ s for each of the 50 interactions, resulting in a total simulation time of  $> 1$  ms. These computations are the longest and most exhaustive PMF computations of amino acid interactions in non-natural solvents to date and the first to investigate the effects of aIL in detail. In contrast to previous PMF computations of pairwise residue interactions usually employing ps-long windows and few additional replicas, resulting in ns timescale trajectories<sup>58, 59, 62, 63, 160, 185</sup>, we employ long simulation times of 3  $\mu$ s per interaction for each of the seven solvents with 16 replicas. In doing so, we demonstrated that, while the interactions in water usually converge on the sub-ns timescale, the effects of aIL occur on the super-ns timescale. Hence, the extended simulation times allowed us to obtain statistically converged results for specific aIL effects, including perturbation and stabilization effects occurring on longer timescales<sup>34</sup> (see **Figure S1** and **Text S1**). In this regard, we previously showed that interactions of aIL and salt ions with protein surface residues with negative binding free energies converge ( $\Delta(\Delta G^0_{\text{final}} - \Delta G^0(t)) \leq 0.5 \text{ kcal mol}^{-1}$ ) within 100 ns, whereas interactions with positive binding free energies require up to 600 ns<sup>34</sup>. Our results indicate that the high solvent-accessibility of the isolated amino acids compared to protein surface residues in conjunction with the higher concentration of up to 2.0 M and the high number of replicas still enable us to obtain statistically converged results for most interactions and effects despite a "short" simulation time of 10 ns per replica per window. Additionally, the high density of windows at higher distances revealed detailed solvent bridge-like effects up to the second SSM and distances of up to 10 Å, as observed for many  $\pi$ -stacking interactions.

We used the well-established AMBER ff14SB and GAFF force fields<sup>186, 187</sup> and the OPC water model<sup>188</sup> with IL ion parameters derived using the RESP procedure<sup>189</sup>, which reproduce physicochemical equilibrium and transport properties of IL and aIL well<sup>34, 190</sup> and were successfully employed by us previously in this combination for the same aIL in similar concentration ranges<sup>34</sup>. For a detailed evaluation of the accuracy of the force field and water model combination in reproducing IL and aIL properties, we refer to the above-mentioned studies. We note that non-polarizable force fields using fixed partial charges may overstabilize attractive solute-solute interactions<sup>191-195</sup>, and explicitly including polarizability is considered more accurate, particularly for the simulation of highly concentrated aIL<sup>34, 195, 196</sup>. Yet, in particular because of the potentially long convergence times highlighted above, we decided on using non-polarizable force fields, allowing us to exploit the higher computational efficiency of such force fields *versus* polarizable ones<sup>195</sup> to obtain increased sampling. Computationally more efficient corrections, such as the NBFIX<sup>194</sup> or ECC<sup>197</sup> approaches, were shown to improve simulation accuracy for many systems<sup>193, 194, 196, 198-203</sup> and, e.g., to substantially destabilize the bound state pairwise interactions of opposite-charged ions<sup>194</sup>. However, their effects can be system- and force field-specific<sup>204</sup>, making them potentially unpredictable to use without previous extensive testing.

We decided to employ a full-atomistic description of the solvent in contrast to implicit continuum solvent models, such as the Poisson Boltzmann (PB) model<sup>205</sup>, the Generalized Born (GB) model<sup>206, 207</sup>, the Effective Energy Function (EEF1) model<sup>208</sup>, or the uniform dielectric constant model ( $\epsilon = 80$ ), which were previously employed to calculate PMF profiles of pairwise amino acid interactions in water and compared to PMF profiles from explicit MD simulations<sup>58, 209-211</sup>. The PB and GB models often, yet not always,<sup>58</sup> provided an accurate description of forces at interaction contact minima but also often failed to correctly describe other local minima and maxima, particularly the global maximum, resulting in an overall performance unpractical for the description of interaction PMFs<sup>58, 209-211</sup>. Both models miss, among other things, effects due to the finite sizes of the solvent/electrolyte molecules<sup>212</sup>, which leads to effects such as like-charge attraction not being covered<sup>58</sup>, in contrast to what we observe when using an explicit solvent. In turn, in addition to similar reports<sup>131, 213, 214</sup>, Geney *et al.*<sup>62</sup> showed that the GB continuum solvent models overstabilized salt bridges by as much as 4 kcal mol<sup>-1</sup>. Furthermore, GB models were shown to form incorrect salt bridges in place of hydrophobic contacts, overstabilizing certain conformations<sup>215, 216</sup>. In addition, we decided to simulate fully capped amino acid residues in contrast to zwitterionic amino acids or side-chain analogs, which can reduce the complexity of the simulation setup. However, particularly for charged and polar amino acids, self-solvation and solvent-exclusion effects result in substantial differences in solvation free energies of zwitterionic amino acids or side-chain analogs compared to capped amino acids<sup>78, 122-125</sup>.

We restrained the relative orientations of our systems using angle and dihedral restraints, which similarly were previously successfully used in PMF computations of ligand association to proteins<sup>217</sup>. The restraints effectively reduce the conformational space that the residues can adapt to the region of interest, i.e., the restricted association and dissociation processes mimic the conditions on protein surfaces but disallows deriving absolute binding free energies from the PMFs without the application of non-trivial approaches, such

as the double-decoupling scheme<sup>218-220</sup>. Note that due to the different restraints for each sampled conformation, comparisons between different orientations should be made with care. However, our results at least allow for a qualitative comparison in such cases and for quantitative comparisons between solvents and residue pairs in the same orientation.

Overall, our results are in excellent qualitative and quantitative agreement with results from QM studies and other publications reporting comparable PMF profiles of pairwise amino acid interactions (see **Table 1** for comparisons with available literature data). Further, they often are supported by independent observations of specific amino acid interactions or arrangements from other studies and experiments, as, e.g., given for the stable interaction mode of Arg<sup>+</sup>-Arg<sup>+</sup> in protein structures<sup>61, 134</sup>, the disruption of salt bridges caused by the accumulation of [Na<sup>+</sup>] near carboxylic groups at high concentrations of [Na/Cl]<sup>36, 221</sup>, the disruption of  $\pi$ -stacking interactions by [BMIM<sup>+</sup>] ions<sup>34, 35</sup>, the abundant occurrence of methionine-aromatic stacking interactions in protein structures<sup>222</sup>, and the stable arrangement of carboxyl moieties in the presence of [Na/Cl]<sup>138</sup>.

In this regard, we observed strong and distinct effects of salt solutions and aIL on the interactions of both opposite- and like-charged residue pairs, where both solvents stabilized like-charged residue pairs, but only the salt solutions containing [Na<sup>+</sup>] and not [BMIM<sup>+</sup>]-based aIL destabilized opposite-charged residue pairs, i.e., salt bridges. For [Na<sup>+</sup>] ions, this stabilizing effect was previously suggested for various carboxylate- or glutamate-containing systems in experimental<sup>138-141</sup> and computational<sup>138, 140, 141, 221, 223</sup> studies, respectively. The stabilization was attributed to the specific binding properties of [Na<sup>+</sup>] due to the "law of matching water affinities"<sup>224, 225</sup> and non-specific charge screening effects<sup>226, 227</sup>. For U-shaped EDTA<sup>4-</sup> aggregates encompassing [Na<sup>+</sup>] ions between their carboxylate groups<sup>138</sup>, this effect was suggested to exceed unbeneficial hydrophobic solvation<sup>228, 229</sup> of the ethylene moieties and, thus, stabilize the conformation. Here, we demonstrate that [BMIM<sup>+</sup>] can induce similar effects in pairwise like-charged residue interactions mediated by preferential interactions with carboxylate moieties and unspecific charge screening effects, revealing the thermodynamic basis for [BMIM<sup>+</sup>]-induced structural conformation changes. The electrostatic nature of this effect suggests that it can also occur in other aIL with similar or stronger affinities for carboxylate moieties. In contrast to like-charged interactions, [BMIM<sup>+</sup>] led to a minor stabilization of opposite-charged interactions, whereas [Na<sup>+</sup>] destabilized them. Destabilizing effects and the accumulations of [Na<sup>+</sup>] around negatively-charged moieties were indicated previously<sup>221</sup>, whereas they were not yet described for [BMIM<sup>+</sup>] ions. However, a lack of destabilization due to [BMIM<sup>+</sup>] agrees with studies that observed no destabilizing effects for alkali metal cations larger than [Na<sup>+</sup>]<sup>221, 230</sup>. Overall, the stabilizing effect of [BMIM<sup>+</sup>] might seem to contradict the notion that the strength of salt bridges should decrease with increasing strength according to the Debye-Hückel equation<sup>132, 231</sup>. However, the effect of increasing ionic strength on salt bridge strength was case-dependent for many salt bridges<sup>210</sup>. In our case, we can determine the effect to be anion-based, albeit the cation determines whether the effect can occur, as [Na<sup>+</sup>] displaces [Cl<sup>-</sup>] from the interface due to preferential

interactions with Glu<sup>-</sup>, whereas [BMIM<sup>+</sup>] allows for the accumulation of [Cl<sup>-</sup>] ions at the residue interface. Overall, we attribute the stabilizing effect to a reduced desolvation penalty upon salt bridge association mediated by the weak chaotropic nature of [Cl<sup>-</sup>], inducing a weak water structure-breaking<sup>133</sup>. However, the solvation dynamics of ILs and water are extremely complex and depend on many properties of ILs<sup>232-234</sup>, and a definite explanation requires further investigations. Our PMF profiles of isolated amino acid pairs, based on long simulation times and statistically converged computations, enabled us to capture these effects, whereas this was not visible in previous studies, likely caused by high noise or too short simulation times<sup>36, 58</sup>.

From our description of PMF profiles of intramolecular amino acid interactions in water, aIL, and salt solutions, implications for rational mutagenesis approaches can be derived. E.g., in  $\pi$ - $\pi$ -stacking systems, the His-His interaction remained stable in [BMIM<sup>+</sup>]-based aIL in contrast to interactions involving other aromatic residues. Hence, substituting solvent-exposed residues for His-His interactions might be an efficient way to improve enzyme resistance to these aIL. These results can only partially be applied to other aIL than [BMIM<sup>+</sup>]-based ones, as structural changes in IL ions can result in different effects on residue interactions. While [BMIM<sup>+</sup>]-based aIL belong to the most frequently employed ILs, an immense variety of IL exists<sup>235</sup>. According to our simulations (~150 ns/day on an Nvidia A100 GPU), computation of a PMF for one additional solvent at a given concentration will require ~20 days of US simulation time on a single current high-performance GPU, although these computations are trivially parallelizable.

In summary, using a comprehensive dataset of computed PMF profiles for representative pairwise protein residue interactions, we show that incubation in aIL and salt solutions can induce substantial residue-, conformation-, solvent-, concentration-, and distance-dependent effects on intramolecular interactions. These effects can be destabilizing or stabilizing with differences of more than 3 kcal mol<sup>-1</sup> in the PMFs and result from the complex interplay of competitive or cooperative noncovalent ion-residue interactions, changes in solvent structural dynamics, or unspecific charge screening effects. As a result, aIL and salt solutions can promote non-native intramolecular interactions in proteins, such as like-charged interactions of Glu<sup>-</sup>-Glu<sup>-</sup> residue pairs or solvent-separated  $\pi$ - $\pi$ -stacking interactions, ultimately resulting in conformational changes in the local protein structure<sup>16, 30, 34, 35, 41</sup>. These structural changes, e.g., the [TfO<sup>-</sup>]-induced transition of the catalytic gate from the open to the closed state in *Candida antarctica* Lipase B<sup>30</sup>, or the [BMIM<sup>+</sup>]-induced disruption of the H3-W31  $\pi$ - $\pi$ -stacking interaction in *Bacillus subtilis* Lipase A<sup>35</sup>, can greatly affect activity or stability of enzymes, which may result in enzyme performances impractical for biotechnological approaches. *Vice versa*, such complex effects may be exploited in rational residue substitutions to improve enzyme performance. Effects might be even more complex when more ion species are involved or when more than two residues interact. Our findings stress the need to consider explicit and implicit effects of aIL incubation on intramolecular interactions when employing computational tools to estimate effects on protein stability upon rational mutagenesis targeting such solvents.

## 5 Materials and Methods

### 5.1 System preparation for molecular dynamics simulations

To investigate the dissociation/association process of isolated amino acid pairs in aIL and salt solutions, we performed all-atom US simulations of pairwise pre-oriented amino acids with increasing distance. The structural dynamics of these interactions were investigated in the commonly employed aIL ([BMIM/Cl] and [BMIM/TfO])<sup>12</sup> and [Na/Cl] solutions (see **Table 2** for an overview of all systems). To determine the concentration-specific effects of these solvents, we employed biotechnologically relevant concentrations of 0.2 M and 2 M, covering two orders of magnitude, which can lead to significant inhibition of enzymes<sup>12</sup>. Finally, we performed US simulations in pure water, which served as a control. For each interaction in each solvent, 16 replicas per sampled US window were used.

**Table 2: Cation types and concentrations of investigated aqueous solutions.**

	MD00 <sup>[a]</sup>	MD01	MD02	MD03	MD04	MD05	MD06
<b>Cation</b>	-	[BMIM <sup>+</sup> ]	[BMIM <sup>+</sup> ]	[Na <sup>+</sup> ]	[BMIM <sup>+</sup> ]	[BMIM <sup>+</sup> ]	[Na <sup>+</sup> ]
<b>Anion</b>	-	[Cl <sup>-</sup> ]	[TfO <sup>-</sup> ]	[Cl <sup>-</sup> ]	[Cl <sup>-</sup> ]	[TfO <sup>-</sup> ]	[Cl <sup>-</sup> ]
<b>Conc.</b> <sup>[b]</sup>	-	0.2	0.2	0.2	2.0	2.0	2.0

<sup>[a]</sup> Pure water. In the case of charged amino acids, [Na<sup>+</sup>] or [Cl<sup>-</sup>] were used as counterions to neutralize the system.

<sup>[b]</sup> Concentration, in M.

As reaction coordinate, the COM distance of the functional groups of both amino acids was chosen, as done before<sup>236</sup>. For the definition of functional groups for each residue following the Amber ff14SB force field<sup>186</sup> atom naming scheme, see **Table 3**. We applied US windows from a distance of 3 Å to a distance of 12 Å interspaced by 0.5 Å; the largest distance sufficed to reach an unbound state for all interactions; no PMF profile showed changes beyond 0.1 kcal mol<sup>-1</sup> from 11.5 Å to 12.0 Å. US potentials with force constants of 10 kcal mol<sup>-1</sup> Å<sup>-2</sup> were applied to restrain the COM distances to the reference values.

**Table 3: Atoms representing functional groups of amino acids**

Res	Atoms	Res	Atoms	Res	Atoms	Res	Atoms
A	CB	D	OD1, OD2	I	CB, CG1, CG2, CD1	F	CG, CD1, CD2, CE1, CE2, CZ
G	CA	E	OG1, OG2	T	CB, OG1, CG2	H	CG, ND1, CD2, CE1, NE2
K	NZ	N	ND2, OD1	P	CB, CG, CD	W	CG, CD1, CD2, NE1, CE2, CE3, CZ2, CZ3, CH
C	SG	Q	NE1, OE1	V	CB, CG1, CG2	Y	CG, CD1, CD2, CE1, CE2, CZ, OH
S	OG	R	NH1, NH2 (, NE)	M	CE, SD, CG, CB	L	CB, SG, CD1, CD2

The relative orientation of the two residues was given using additional restraints with force constants of  $500 \text{ kcal mol}^{-1} \text{ rad}^{-2}$  applied in harmonic restraints. Schematic representations displaying the atom groups of the local reference structures used to construct the restraint settings are shown in **Figure 4** for all orientations. Additionally, the side-chain torsion angles were restrained to their reference positions using lower force constants of  $50 \text{ kcal mol}^{-1} \text{ rad}^{-2}$ , also applied in harmonic restraints. Finally, the position of the first residue was fixed in space on its initial Cartesian coordinates using harmonic restraints with force constants of  $10 \text{ kcal mol}^{-1} \text{ \AA}^{-2}$ .

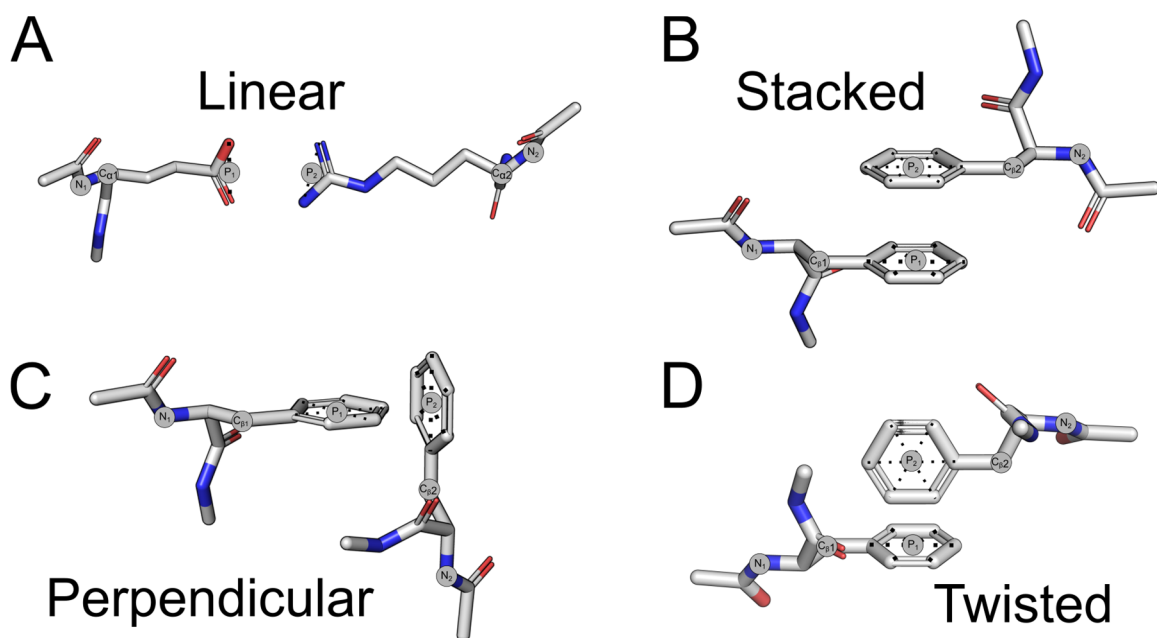


**Figure 4:** Overview of restraints used to preserve the relative orientation of the residues. (A) Linear orientation. The relative orientation of both residues was preserved using the two angles  $C_{\alpha 1}-P_1-P_2$  and  $C_{\alpha 1}-P_1-C_{\alpha 2}$ . (B) Stacked orientation. The relative orientation of both residues was preserved using the two angles  $C_{\beta 1}-P_1-P_2$  and  $P_1-P_2-C_{\beta 2}$ , as well as three dihedral angles  $C_{\beta 1}-P_1-P_2-C_{\beta 2}$ ,  $P_1-P_2-C_{\beta 2}-N_2$ , and  $N_1-C_{\beta 1}-P_1-P_2$ . (C) Perpendicular orientation. The relative orientation of both residues was preserved using the two angles  $C_{\beta 1}-P_1-P_2$  and  $P_1-P_2-C_{\beta 2}$ , as well the dihedral angle  $N_1-C_{\beta 1}-P_1-P_2$ . (D) Twisted orientation. The relative orientation

of both residues was preserved using the two angles  $C_{\beta 1}-P_1-P_2$  and  $P_1-P_2-C_{\beta 2}$ , as well as two dihedral angles  $C_{\beta 1}-P_1-P_2-C_{\beta 2}$  and  $P_1-P_2-C_{\beta 2}-N_2$ , and an additional dihedral angle comprising  $N_1-C_{\beta 1}-P_1$  and one atom of the side of the aromatic moieties of the second residue.

For initial configurations, we placed two pre-oriented amino acids with the functional groups facing each other in the simulation box at the respective distance. We used ACE/NME capping groups to avoid artificially charged N- and C-termini. We used Packmol<sup>237</sup> and Packmol-Memgen<sup>238</sup> to randomly place the needed amount of cations and anions in the simulation box to fit the concentration of the respective ionic liquid or salt solution. Additional cations or anions were added in the case of charged amino acids to ensure the neutrality of the system. The systems were then solvated using the OPC water model<sup>188</sup>, also using Packmol<sup>237</sup>. In all cases, periodic boundary conditions were used. The size of the systems is between  $\sim 16,000$  to  $\sim 25,000$  atoms. All systems had at least a 12 Å distance between the residues and the box boundaries to prevent self-interaction of the amino acids across the box borders. All hydrogen atoms of the structures were removed using the REDUCE program<sup>239</sup> and reassigned with the program LEaP<sup>240</sup> according to the Amber ff14SB library<sup>186</sup>, which is included in the AMBER18 program package<sup>241</sup>. The atomic partial charges and force field parameters were taken from the Amber ff14SB force field<sup>186</sup>. The preparation of the IL ions has been described before<sup>34</sup>. In short, the initial 3D structures were prepared using LEaP<sup>240</sup> from AMBER18<sup>241</sup>. The initial structures were subjected to quantum mechanical (QM) geometry optimization using Gaussian 16<sup>242</sup> at the HF/6-31G\* level of theory<sup>243</sup>. The QM-optimized structures were used as starting structures for MD simulations. Atomic partial charges for IL were derived according to the RESP procedure<sup>189</sup> (see **Figure S15** in ref. <sup>34</sup>). The force field parameters for IL were taken from the general amber force field (GAFF)<sup>187</sup>.

## 5.2 Molecular dynamics simulations

The MD simulations were performed following ref. <sup>244</sup>. For all thermalization and relaxation steps, the relative orientation of the amino acids was fixed. The systems were first subjected to energy minimization to eliminate steric clashes. Here, harmonic restraints with force constants of 10 kcal mol<sup>-1</sup> Å<sup>-2</sup> were applied to all residue atoms (excluding the ACE/NME caps) for 25000 cycles (20000 cycles steepest descent (SD) followed by 5000 cycles conjugate gradient (CG) minimization).

In the subsequent thermalization, the system was first heated from 0 K to 50 K over 25 ps in a canonical (NVT) MD simulation. The same harmonic restraints were applied as in the equilibration steps, and a time step of 1 fs was used. The temperature was then raised from 100 K to 300 K over 80 ps of isobaric-isothermal (NPT) MD simulations. Subsequently, the density was adapted to 1 g cm<sup>-3</sup> over 10 ps of NPT-MD simulations. Finally, the system was relaxed over the course of six NVT-MD simulations with a total length of 400 ps with time steps increasing from 1 fs to 4 fs. Here, the harmonic restraints of the first and second residue were changed to 25 and 0 kcal mol<sup>-1</sup> Å<sup>-2</sup>, respectively, and the relative orientations were switched on (see above). In all MD simulations, the particle mesh Ewald (PME) method<sup>245</sup> was used to treat long-range electrostatic

interactions. The distance cutoff for short-range non-bonded interactions was set to 9 Å. Langevin dynamics were used with a time constant ( $\tau$ ) of 0.5 ps for heat bath-coupling to keep the system temperature at the target temperature of 300.0 K during the simulations. The Berendsen barostat<sup>246</sup> was used for NPT ensembles. The SHAKE<sup>247</sup> algorithm was applied to all bonds involving hydrogens. To set up sixteen independent MD production simulations for each US window, starting velocities were assigned at random.

US simulations were then performed in an NPT ensemble at 300.0 K with the Berendsen barostat<sup>246</sup> for 10 ns using the AMBER18 package<sup>241</sup>. See above for the range of the reaction coordinate and the force constant of the US potentials. The SHAKE algorithm<sup>247</sup> was applied to constrain bond lengths of hydrogen atoms. For efficient sampling, the hydrogen mass repartitioning strategy<sup>248</sup> was applied, which allows a 4 fs-time step for the integration of Newton's equation of motions. Long-range electrostatic interactions were taken into account using the AMBER GPU implementation of the Particle Mesh Ewald (PME) algorithm<sup>245</sup> with a distance cutoff for short-range non-bonded interactions of 9 Å and a charge grid size of 64 units for all dimensions. Coordinates were saved every 40 ps. Distances, angles, and dihedral values of the reaction coordinate and different restraints were saved every 0.5 ps. For further, more detailed information on all simulation parameters, we refer to the template input files for the thermalization and production runs provided in the SI. For default values used, please see the AMBER18 manual.

The simulation results were post-processed using the fast, memory-efficient weighted histogram analysis method (WHAM)<sup>249</sup> to generate 16 individual PMF profiles with a step size of 0.04 Å, resulting in 250 data points from 2.0 Å to 12.0 Å. All individual PMF profiles were anchored to a value of 0 kcal mol<sup>-1</sup> at the final separation distance of 12.0 Å, i.e., the completely unbound state. The 16 individual PMF profiles were then used to compute the mean  $\pm$  standard error of the mean, resulting in the final PMF profile shown in the main text. The significance of differences between PMFs at each of the 250 data points between water and aIL/salt solutions was assessed using the two-sided independent Student's *t*-test. Results with *p*-values < 0.05 were considered significant.

### 5.3 Trajectory analysis

Structural analyses were performed with *cpptraj*<sup>250</sup> from the AmberTools18 package<sup>241</sup> on conformations from the US simulations. The following measures were evaluated: I) the root-mean-square deviation (RMSD) of all non-hydrogen atoms of the second residue after alignment to the first residue as a measure of structural similarity to the starting structure, and II) solvent density grids to display the locations of aIL interaction sites at the protein residues, using a grid spacing of 1 Å.



## 6 Acknowledgments

This work was supported by the Juelich-Aachen Research Alliance Center for Simulation and Data Science (JARA-CSD) School for Simulations and Data Science (SSD). Parts of the study were supported by the German Federal Ministry of Education and Research (BMBF) through funding number 031B0837A "LipoBiocat" to H.G., the German Research Foundation (DFG) through funding no. INST 208/704-1 FUGG to H.G., as well as the state of North-Rhine Westphalia (NRW) and the European Regional Development Fund (EFRE) through funding no. 34-EFRE-0300096 "CLIB-Kompetenzzentrum Biotechnologie (CKB)" to H.G.. We are grateful for computational support and infrastructure provided by the "Zentrum für Informations- und Medientechnologie" (ZIM) at the Heinrich Heine University Düsseldorf and the computing time provided by the John von Neumann Institute for Computing (NIC) to H.G. on the supercomputer JUWELS at Jülich Supercomputing Centre (JSC) (user ID: HKF7, VSK33, protil).

## **7 Author contributions**

HG designed the study. TEH performed computations. TEH and HG analyzed the data. TEH and HG wrote the manuscript.

## **8 Declaration of interest**

The authors declare no competing interests.

## 9 Data and software availability

For molecular simulations, the AMBER18 package of molecular simulation codes was used. AMBER18 is available from <http://ambermd.org/>. The data generated in the course of this work is available in the Supporting Information: I) Data of PMF profiles averaged over the 16 replica shown in the manuscript and the Supporting Information as presented in the figures (file PMFdata\_average.txt); II) Raw data of the individual PMF profiles obtained for the 16 replica (file PMFdata\_replica.txt).

## 10 Supporting information

Supporting Information Available:

- Evaluation of the simulation setup, further discussions of our results in view of available literature additionally to the main text, and plots of all other PMF profiles not shown in the main text (file SI\_rev\_final.pdf).
- Data of PMF profiles averaged over the 16 replica shown in the manuscript and the Supporting Information as presented in the figures (file PMFdata\_average.txt).
- Raw data of the individual PMF profiles obtained for the 16 replica (file PMFdata\_replica.txt).

## 11 References

1. Barrett, G. C.; Elmore, D. T., *Amino Acids and Peptides*. Cambridge University Press: 1998.
2. Pfleger, C.; Rath, P. C.; Klein, D. L.; Radestock, S.; Gohlke, H., Constraint Network Analysis (CNA): A Python Software Package for Efficiently Linking Biomacromolecular Structure, Flexibility, (Thermo-)Stability, and Function. *J. Chem. Inf. Model.* **2013**, *53*, 1007-1015.
3. Schymkowitz, J.; Borg, J.; Stricher, F.; Nys, R.; Rousseau, F.; Serrano, L., The Foldx Web Server: An Online Force Field. *Nucleic Acids Res.* **2005**, *33*, W382-388.
4. Leaver-Fay, A.; Tyka, M.; Lewis, S. M.; Lange, O. F.; Thompson, J.; Jacak, R.; Kaufman, K.; Renfrew, P. D.; Smith, C. A.; Sheffler, W.; Davis, I. W.; Cooper, S.; Treuille, A.; Mandell, D. J.; Richter, F.; Ban, Y. E.; Fleishman, S. J.; Corn, J. E.; Kim, D. E.; Lyskov, S.; Berrondo, M.; Mentzer, S.; Popovic, Z.; Havranek, J. J.; Karanicolas, J.; Das, R.; Meiler, J.; Kortemme, T.; Gray, J. J.; Kuhlman, B.; Baker, D.; Bradley, P., Rosetta3: An Object-Oriented Software Suite for the Simulation and Design of Macromolecules. *Methods Enzymol.* **2011**, *487*, 545-574.
5. Cheng, C. Y.; Chou, F.-C.; Das, R. Modeling Complex Rna Tertiary Folds with Rosetta. In *Methods Enzymol.*; Elsevier: 2015; Vol. 553, pp 35-64.
6. Conchúir, S. Ó.; Barlow, K. A.; Pache, R. A.; Ollikainen, N.; Kundert, K.; O'Meara, M. J.; Smith, C. A.; Kortemme, T., A Web Resource for Standardized Benchmark Datasets, Metrics, and Rosetta Protocols for Macromolecular Modeling and Design. *PLoS One* **2015**, *10*, e0130433.
7. Ovchinnikov, S.; Kinch, L.; Park, H.; Liao, Y. X.; Pei, J. M.; Kim, D. E.; Kamisetty, H.; Grishin, N. V.; Baker, D., Large-Scale Determination of Previously Unsolved Protein Structures Using Evolutionary Information. *eLife* **2015**, *4*, e09248.
8. Cui, H.; Cao, H.; Cai, H.; Jaeger, K. E.; Davari, M. D.; Schwaneberg, U., Computer-Assisted Recombination (Compassr) Teaches Us How to Recombine Beneficial Substitutions from Directed Evolution Campaigns. *Chemistry* **2020**, *26*, 643-649.
9. Cui, H.; Jaeger, K. E.; Davari, M. D.; Schwaneberg, U., Compassr Fields Highly Organic-Solvent-Tolerant Enzymes through Recombination of Compatible Substitutions. *Chemistry* **2021**, *27*, 2789-2797.
10. Cui, H.; Pramanik, S.; Jaeger, K.-E.; Davari, M. D.; Schwaneberg, U., Compassr-Guided Recombination Unlocks Design Principles to Stabilize Lipases in IIs with Minimal Experimental Efforts. *Green Chem.* **2021**, *23*, 3474-3486.
11. El Harrar, T.; Davari, M. D.; Jaeger, K.-E.; Schwaneberg, U.; Gohlke, H., Critical Assessment of Structure-Based Approaches to Improve Protein Resistance in Aqueous Ionic Liquids by Enzyme-Wide Saturation Mutagenesis. *Comput. Struct. Biotechnol. J.* **2021**, *20*, 399-409.
12. Frauenkron-Machedjou, V. J.; Fulton, A.; Zhu, L.; Anker, C.; Bocola, M.; Jaeger, K. E.; Schwaneberg, U., Towards Understanding Directed Evolution: More Than Half of All Amino Acid Positions Contribute to Ionic Liquid Resistance of Bacillus Subtilis Lipase A. *ChemBioChem* **2015**, *16*, 937-945.
13. Guerois, R.; Nielsen, J. E.; Serrano, L., Predicting Changes in the Stability of Proteins and Protein Complexes: A Study of More Than 1000 Mutations. *J. Mol. Biol.* **2002**, *320*, 369-387.
14. Datta, S.; Holmes, B.; Park, J. I.; Chen, Z. W.; Dibble, D. C.; Hadi, M.; Blanch, H. W.; Simmons, B. A.; Sapra, R., Ionic Liquid Tolerant Hyperthermophilic Cellulases for Biomass Pretreatment and Hydrolysis. *Green Chem.* **2010**, *12*, 338-345.
15. Jaeger, V.; Burney, P.; Pfaendtner, J., Comparison of Three Ionic Liquid-Tolerant Cellulases by Molecular Dynamics. *Biophys. J.* **2015**, *108*, 880-892.
16. Kaar, J. L.; Jesionowski, A. M.; Berberich, J. A.; Moulton, R.; Russell, A. J., Impact of Ionic Liquid Physical Properties on Lipase Activity and Stability. *J. Am. Chem. Soc.* **2003**, *125*, 4125-4131.
17. Nordwald, E. M.; Brunecky, R.; Himmel, M. E.; Beckham, G. T.; Kaar, J. L., Charge Engineering of Cellulases Improves Ionic Liquid Tolerance and Reduces Lignin Inhibition. *Biotechnol. Bioeng.* **2014**, *111*, 1541-1549.
18. Turner, M. B.; Spear, S. K.; Huddleston, J. G.; Holbrey, J. D.; Rogers, R. D., Ionic Liquid Salt-Induced Inactivation and Unfolding of Cellulase from *Trichoderma Reesei*. *Green Chem.* **2003**, *5*, 443-447.
19. Zhao, H.; Jones, C. L.; Baker, G. A.; Xia, S.; Olubajo, O.; Person, V. N., Regenerating Cellulose from Ionic Liquids for an Accelerated Enzymatic Hydrolysis. *J. Biotechnol.* **2009**, *139*, 47-54.
20. Jacob, M.; Geeves, M.; Holtermann, G.; Schmid, F. X., Diffusional Barrier Crossing in a Two-State Protein Folding Reaction. *Nat. Struct. Biol.* **1999**, *6*, 923-926.
21. Zhang, X.; Beuron, F.; Freemont, P. S., Machinery of Protein Folding and Unfolding. *Curr. Opin. Struct. Biol.* **2002**, *12*, 231-238.
22. Summers, S.; Kraft, C.; Alamdari, S.; Pfaendtner, J.; Kaar, J. L., Enhanced Activity and Stability of *Acidothermus Cellulolyticus* Endoglucanase 1 in Ionic Liquids Via Engineering Active Site Residues and Non-Native Disulfide Bridges. *ACS Sustainable Chem. Eng.* **2020**, *8*, 11299-11307.

23. De Diego, T.; Lozano, P.; Gmouh, S.; Vaultier, M.; Iborra, J. L., Fluorescence and Cd Spectroscopic Analysis of the A-Chymotrypsin Stabilization by the Ionic Liquid, 1-Ethyl-3-Methylimidazolium Bis [(Trifluoromethyl) Sulfonyl] Amide. *Biotechnol. Bioeng.* **2004**, *88*, 916-924.
24. Summers, C. A.; Flowers, R. A., Protein Renaturation by the Liquid Organic Salt Ethylammonium Nitrate. *Protein Sci.* **2000**, *9*, 2001-2008.
25. Yamamoto, E.; Yamaguchi, S.; Nagamune, T., Protein Refolding by N-Alkylpyridinium and N-Alkyl-N-Methylpyrrolidinium Ionic Liquids. *Appl. Biochem. Biotechnol.* **2011**, *164*, 957-967.
26. Rawat, K.; Bohidar, H., Universal Charge Quenching and Stability of Proteins in 1-Methyl-3-Alkyl (Hexyl/Octyl) Imidazolium Chloride Ionic Liquid Solutions. *J. Phys. Chem. B* **2012**, *116*, 11065-11074.
27. Figueiredo, A. M.; Sardinha, J.; Moore, G. R.; Cabrita, E. J., Protein Destabilisation in Ionic Liquids: The Role of Preferential Interactions in Denaturation. *Phys. Chem. Chem. Phys.* **2013**, *15*, 19632-19643.
28. Jaeger, V. W.; Pfandtner, J., Structure, Dynamics, and Activity of Xylanase Solvated in Binary Mixtures of Ionic Liquid and Water. *ACS Chem. Biol.* **2013**, *8*, 1179-1186.
29. Magnuson, D. K.; Bodley, J. W.; Evans, D. F., The Activity and Stability of Alkaline-Phosphatase in Solutions of Water and the Fused Salt Ethylammonium Nitrate. *J. Solution Chem.* **1984**, *13*, 583-587.
30. Kim, H. S.; Eom, D.; Koo, Y. M.; Yingling, Y. G., The Effect of Imidazolium Cations on the Structure and Activity of the *Candida Antarctica* Lipase B Enzyme in Ionic Liquids. *Phys. Chem. Chem. Phys.* **2016**, *18*, 22062-22069.
31. Machado, M. F.; Queiros, R. P.; Santos, M. D.; Fidalgo, L. G.; Delgadillo, I.; Saraiva, J. A., Effect of Ionic Liquids Alkyl Chain Length on Horseradish Peroxidase Thermal Inactivation Kinetics and Activity Recovery after Inactivation. *World J. Microbiol. Biotechnol.* **2014**, *30*, 487-494.
32. Takekiyo, T.; Yamazaki, K.; Yamaguchi, E.; Abe, H.; Yoshimura, Y., High Ionic Liquid Concentration-Induced Structural Change of Protein in Aqueous Solution: A Case Study of Lysozyme. *J. Phys. Chem. B* **2012**, *116*, 11092-11097.
33. Lange, C.; Patil, G.; Rudolph, R., Ionic Liquids as Refolding Additives: N'-Alkyl and N'-( $\Omega$ -Hydroxyalkyl) N-Methylimidazolium Chlorides. *Protein Sci.* **2005**, *14*, 2693-2701.
34. El Harrar, T.; Frieg, B.; Davari, M. D.; Jaeger, K.-E.; Schwaneberg, U.; Gohlke, H., Aqueous Ionic Liquids Redistribute Local Enzyme Stability Via Long-Range Perturbation Pathways. *Comput. Struct. Biotechnol. J.* **2021**, *19*, 4248-4264.
35. Nordwald, E. M.; Plaks, J. G.; Snell, J. R.; Sousa, M. C.; Kaar, J. L., Crystallographic Investigation of Imidazolium Ionic Liquid Effects on Enzyme Structure. *ChemBioChem* **2015**, *16*, 2456-2459.
36. Pylaeva, S.; Brehm, M.; Sebastiani, D., Salt Bridge in Aqueous Solution: Strong Structural Motifs but Weak Enthalpic Effect. *Sci. Rep.* **2018**, *8*, 13626.
37. Abdelhamid, R. F.; Obara, Y.; Uchida, Y.; Kohzuma, T.; Dooley, D. M.; Brown, D. E.; Hori, H., Pi-Pi Interaction between Aromatic Ring and Copper-Coordinated His81 Imidazole Regulates the Blue Copper Active-Site Structure. *J. Biol. Inorg. Chem.* **2007**, *12*, 165-173.
38. Singh, O.; Lee, P. Y.; Matysiak, S.; Bermudez, H., Dual Mechanism of Ionic Liquid-Induced Protein Unfolding. *Phys. Chem. Chem. Phys.* **2020**, *22*, 19779-19786.
39. Nordwald, E. M.; Armstrong, G. S.; Kaar, J. L., Nmr-Guided Rational Engineering of an Ionic-Liquid-Tolerant Lipase. *Acs Catalysis* **2014**, *4*, 4057-4064.
40. Pramanik, S.; Dhoke, G. V.; Jaeger, K. E.; Schwaneberg, U.; Davari, M. D., How to Engineer Ionic Liquids Resistant Enzymes: Insights from Combined Molecular Dynamics and Directed Evolution Study. *ACS Sustainable Chem. Eng.* **2019**, *7*, 11293-11302.
41. Zhao, J.; Frauenkron-Machedjou, V. J.; Fulton, A.; Zhu, L.; Davari, M. D.; Jaeger, K. E.; Schwaneberg, U.; Bocola, M., Unraveling the Effects of Amino Acid Substitutions Enhancing Lipase Resistance to an Ionic Liquid: A Molecular Dynamics Study. *Phys. Chem. Chem. Phys.* **2018**, *20*, 9600-9609.
42. Cauet, E.; Rooman, M.; Wintjens, R.; Lievin, J.; Biot, C., Histidine-Aromatic Interactions in Proteins and Protein-Ligand Complexes: Quantum Chemical Study of X-Ray and Model Structures. *J. Chem. Theory. Comput.* **2005**, *1*, 472-483.
43. Du, Q. S.; Long, S. Y.; Meng, J. Z.; Huang, R. B., Empirical Formulation and Parameterization of Cation- $\Pi$  Interactions for Protein Modeling. *J. Comput. Chem.* **2012**, *33*, 153-162.
44. Rodriguez-Sanz, A. A.; Cabaleiro-Lago, E. M.; Rodriguez-Otero, J., On the Interaction between the Imidazolium Cation and Aromatic Amino Acids. A Computational Study. *Org. Biomol. Chem.* **2015**, *13*, 7961-7972.
45. Xie, N. Z.; Du, Q. S.; Li, J. X.; Huang, R. B., Exploring Strong Interactions in Proteins with Quantum Chemistry and Examples of Their Applications in Drug Design. *PLoS One* **2015**, *10*, e0137113.
46. Mukherjee, A.; Bhimalapuram, P.; Bagchi, B., Orientation-Dependent Potential of Mean Force for Protein Folding. *J. Chem. Phys.* **2005**, *123*, 014901.

47. Melo, F.; Feytmans, E., Novel Knowledge-Based Mean Force Potential at Atomic Level. *J. Mol. Biol.* **1997**, *267*, 207-222.
48. Debiec, K. T.; Gronenborn, A. M.; Chong, L. T., Evaluating the Strength of Salt Bridges: A Comparison of Current Biomolecular Force Fields. *J. Phys. Chem. B* **2014**, *118*, 6561-6569.
49. White, A. D.; Keefe, A. J.; Ella-Menye, J. R.; Nowinski, A. K.; Shao, Q.; Pfaendtner, J.; Jiang, S., Free Energy of Solvated Salt Bridges: A Simulation and Experimental Study. *J. Phys. Chem. B* **2013**, *117*, 7254-7259.
50. Ahmed, M. C.; Papaleo, E.; Lindorff-Larsen, K., How Well Do Force Fields Capture the Strength of Salt Bridges in Proteins? *PeerJ* **2018**, *6*, e4967.
51. Gallivan, J. P.; Dougherty, D. A., Cation- $\Pi$  Interactions in Structural Biology. *Proc. Natl. Acad. Sci. U. S. A.* **1999**, *96*, 9459-9464.
52. Hassan, S. A., Intermolecular Potentials of Mean Force of Amino Acid Side Chain Interactions in Aqueous Medium. *J. Phys. Chem. B* **2004**, *108*, 19501-19509.
53. Hassan, S. A., Amino Acid Side Chain Interactions in the Presence of Salts. *J. Phys. Chem. B* **2005**, *109*, 21989-21996.
54. Hunter, C. A.; Low, C. M.; Rotger, C.; Vinter, J. G.; Zonta, C., Substituent Effects on Cation- $\Pi$  Interactions: A Quantitative Study. *Proc. Natl. Acad. Sci. U. S. A.* **2002**, *99*, 4873-4876.
55. Anfinsen, C. B., Principles That Govern the Folding of Protein Chains. *Science* **1973**, *181*, 223-230.
56. Anfinsen, C. B.; Haber, E., Studies on the Reduction and Re-Formation of Protein Disulfide Bonds. *J. Biol. Chem.* **1961**, *236*, 1361-1363.
57. Boudon, S.; Wipff, G.; Maigret, B., Monte Carlo Simulations on the Like-Charged Guanidinium-Guanidinium Ion Pair in Water. *J. Phys. Chem.* **1990**, *94*, 6056-6061.
58. Masunov, A.; Lazaridis, T., Potentials of Mean Force between Ionizable Amino Acid Side Chains in Water. *J. Am. Chem. Soc.* **2003**, *125*, 1722-1730.
59. Soetens, J. C.; Millot, C.; Chipot, C.; Jansen, G.; Angyan, J. G.; Maigret, B., Effect of Polarizability on the Potential of Mean Force of Two Cations. The Guanidinium-Guanidinium Ion Pair in Water. *J. Phys. Chem. B* **1997**, *101*, 10910-10917.
60. Vazdar, M.; Heyda, J.; Mason, P. E.; Tesei, G.; Allolio, C.; Lund, M.; Jungwirth, P., Arginine "Magic": Guanidinium Like-Charge Ion Pairing from Aqueous Salts to Cell Penetrating Peptides. *Acc. Chem. Res.* **2018**, *51*, 1455-1464.
61. Vondrasek, J.; Mason, P. E.; Heyda, J.; Collins, K. D.; Jungwirth, P., The Molecular Origin of Like-Charge Arginine-Arginine Pairing in Water. *J. Phys. Chem. B* **2009**, *113*, 9041-9045.
62. Geney, R.; Layten, M.; Gomperts, R.; Hornak, V.; Simmerling, C., Investigation of Salt Bridge Stability in a Generalized Born Solvent Model. *J. Chem. Theory. Comput.* **2006**, *2*, 115-127.
63. Rozanska, X.; Chipot, C., Modeling Ion-Ion Interaction in Proteins: A Molecular Dynamics Free Energy Calculation of the Guanidinium-Acetate Association. *J. Chem. Phys.* **2000**, *112*, 9691-9694.
64. Hénin, J.; Chipot, C., Overcoming Free Energy Barriers Using Unconstrained Molecular Dynamics Simulations. *J. Chem. Phys.* **2004**, *121*, 2904-2914.
65. Yuzlenko, O.; Lazaridis, T., Interactions between Ionizable Amino Acid Side Chains at a Lipid Bilayer-Water Interface. *J. Phys. Chem. B* **2011**, *115*, 13674-13684.
66. Mandell, D. J.; Chorny, I.; Groban, E. S.; Wong, S. E.; Levine, E.; Rapp, C. S.; Jacobson, M. P., Strengths of Hydrogen Bonds Involving Phosphorylated Amino Acid Side Chains. *J. Am. Chem. Soc.* **2007**, *129*, 820-827.
67. Berka, K.; Laskowski, R.; Riley, K. E.; Hobza, P.; Vondrasek, J., Representative Amino Acid Side Chain Interactions in Proteins. A Comparison of Highly Accurate Correlated Ab Initio Quantum Chemical and Empirical Potential Procedures. *J. Chem. Theory. Comput.* **2009**, *5*, 982-992.
68. Makowski, M.; Liwo, A.; Scheraga, H. A., Simple Physics-Based Analytical Formulas for the Potentials of Mean Force of the Interaction of Amino-Acid Side Chains in Water. Vi. Oppositely Charged Side Chains. *J. Phys. Chem. B* **2011**, *115*, 6130-6137.
69. Bikkina, S.; Bhati, A. P.; Padhi, S.; Priyakumar, U. D., Temperature Dependence of the Stability of Ion Pair Interactions, and Its Implications on the Thermostability of Proteins from Thermophiles. *J. Chem. Sci.* **2017**, *129*, 405-414.
70. Makowska, J.; Makowski, M.; Giełdoń, A.; Liwo, A.; Chmurzyński, L., Theoretical Calculations of Heteroconjugation Equilibrium Constants in Systems Modeling Acid-Base Interactions in Side Chains of Biomolecules Using the Potential of Mean Force. *J. Phys. Chem. B* **2004**, *108*, 12222-12230.
71. Muttathukattil, A. N.; Srinivasan, S.; Halder, A.; Reddy, G., Role of Guanidinium-Carboxylate Ion Interaction in Enzyme Inhibition with Implications for Drug Design. *J. Phys. Chem. B* **2019**, *123*, 9302-9311.
72. Thomas, A. S.; Elcock, A. H., Direct Observation of Salt Effects on Molecular Interactions through Explicit-Solvent Molecular Dynamics Simulations: Differential Effects on Electrostatic and Hydrophobic Interactions and Comparisons to Poisson-Boltzmann Theory. *J. Am. Chem. Soc.* **2006**, *128*, 7796-7806.



73. Vaitheeswaran, S.; Thirumalai, D., Interactions between Amino Acid Side Chains in Cylindrical Hydrophobic Nanopores with Applications to Peptide Stability. *Proc. Natl. Acad. Sci. U. S. A.* **2008**, *105*, 17636-17641.
74. Rapp, C.; Klerman, H.; Levine, E.; McClendon, C. L., Hydrogen Bond Strengths in Phosphorylated and Sulfated Amino Acid Residues. *PLoS One* **2013**, *8*, e57804.
75. Makowski, M.; Liwo, A.; Scheraga, H. A., Simple Physics-Based Analytical Formulas for the Potentials of Mean Force of the Interaction of Amino Acid Side Chains in Water. Vii. Charged-Hydrophobic/Polar and Polar-Hydrophobic/Polar Side Chains. *J. Phys. Chem. B* **2017**, *121*, 379-390.
76. Makowski, M.; Liwo, A.; Sobolewski, E.; Scheraga, H. A., Simple Physics-Based Analytical Formulas for the Potentials of Mean Force of the Interaction of Amino-Acid Side Chains in Water. V. Like-Charged Side Chains. *J. Phys. Chem. B* **2011**, *115*, 6119-6129.
77. Allolio, C.; Baxova, K.; Vazdar, M.; Jungwirth, P., Guanidinium Pairing Facilitates Membrane Translocation. *J. Phys. Chem. B* **2016**, *120*, 143-153.
78. No, K. T.; Nam, K.-Y.; Scheraga, H. A., Stability of Like and Oppositely Charged Organic Ion Pairs in Aqueous Solution. *J. Am. Chem. Soc.* **1997**, *119*, 12917-12922.
79. Bootsma, A. N.; Doney, A. C.; Wheeler, S. E., Predicting the Strength of Stacking Interactions between Heterocycles and Aromatic Amino Acid Side Chains. *J. Am. Chem. Soc.* **2019**, *141*, 11027-11035.
80. Chipot, C.; Jaffe, R.; Maigret, B.; Pearlman, D. A.; Kollman, P. A., Benzene Dimer: A Good Model for  $\Pi-\Pi$  Interactions in Proteins? A Comparison between the Benzene and the Toluene Dimers in the Gas Phase and in an Aqueous Solution. *J. Am. Chem. Soc.* **1996**, *118*, 11217-11224.
81. Wheeler, S. E., Understanding Substituent Effects in Noncovalent Interactions Involving Aromatic Rings. *Acc. Chem. Res.* **2013**, *46*, 1029-1038.
82. Makowski, M.; Sobolewski, E.; Czaplewski, C.; Liwo, A.; Oldziej, S.; No, J. H.; Scheraga, H. A., Simple Physics-Based Analytical Formulas for the Potentials of Mean Force for the Interaction of Amino Acid Side Chains in Water. 3. Calculation and Parameterization of the Potentials of Mean Force of Pairs of Identical Hydrophobic Side Chains. *J. Phys. Chem. B* **2007**, *111*, 2925-2931.
83. Ninković, D. B.; Blagojević Filipović, J. P.; Hall, M. B.; Brothers, E. N.; Zarić, S. a. D., What Is Special About Aromatic-Aromatic Interactions? Significant Attraction at Large Horizontal Displacement. *ACS Cent. Sci.* **2020**, *6*, 420-425.
84. Sinnokrot, M. O.; Sherrill, C. D., High-Accuracy Quantum Mechanical Studies of  $\Pi-\Pi$  Interactions in Benzene Dimers. *J. Phys. Chem. A* **2006**, *110*, 10656-10668.
85. Linse, P., Orientation-Averaged Benzene-Benzene Potential of Mean Force in Aqueous Solution. *J. Am. Chem. Soc.* **1993**, *115*, 8793-8797.
86. Sherrill, C. D.; Takatani, T.; Hohenstein, E. G., An Assessment of Theoretical Methods for Nonbonded Interactions: Comparison to Complete Basis Set Limit Coupled-Cluster Potential Energy Curves for the Benzene Dimer, the Methane Dimer, Benzene-Methane, and Benzene-H<sub>2</sub>s. *J. Phys. Chem. A* **2009**, *113*, 10146-10159.
87. Hohenstein, E. G.; Sherrill, C. D., Effects of Heteroatoms on Aromatic  $\Pi-\Pi$  Interactions: Benzene-Pyridine and Pyridine Dimer. *J. Phys. Chem. A* **2009**, *113*, 878-886.
88. Sinnokrot, M. O.; Sherrill, C. D., Highly Accurate Coupled Cluster Potential Energy Curves for the Benzene Dimer: Sandwich, T-Shaped, and Parallel-Displaced Configurations. *J. Phys. Chem. A* **2004**, *108*, 10200-10207.
89. Tsuzuki, S.; Honda, K.; Uchimaru, T.; Mikami, M.; Tanabe, K., Origin of Attraction and Directionality of the  $\Pi/\Pi$  Interaction: Model Chemistry Calculations of Benzene Dimer Interaction. *J. Am. Chem. Soc.* **2002**, *124*, 104-112.
90. Lee, H.; Dehez, F.; Chipot, C.; Lim, H.-K.; Kim, H., Enthalpy-Entropy Interplay in  $\Pi$ -Stacking Interaction of Benzene Dimer in Water. *J. Chem. Theory. Comput.* **2019**, *15*, 1538-1545.
91. Sinnokrot, M. O.; Valeev, E. F.; Sherrill, C. D., Estimates of the Ab Initio Limit for  $\Pi-\Pi$  Interactions: The Benzene Dimer. *J. Am. Chem. Soc.* **2002**, *124*, 10887-10893.
92. Vondrášek, J.; Bendová, L.; Klusák, V.; Hobza, P., Unexpectedly Strong Energy Stabilization inside the Hydrophobic Core of Small Protein Rubredoxin Mediated by Aromatic Residues: Correlated Ab Initio Quantum Chemical Calculations. *J. Am. Chem. Soc.* **2005**, *127*, 2615-2619.
93. Makowski, M.; Sobolewski, E.; Czaplewski, C.; Oldziej, S.; Liwo, A.; Scheraga, H. A., Simple Physics-Based Analytical Formulas for the Potentials of Mean Force for the Interaction of Amino Acid Side Chains in Water. Iv. Pairs of Different Hydrophobic Side Chains. *J. Phys. Chem. B* **2008**, *112*, 11385-11395.
94. Karthikeyan, S.; Nagase, S., Origins of the Stability of Imidazole-Imidazole, Benzene-Imidazole, and Benzene-Indole Dimers: Ccsd (T)/Cbs and Sapt Calculations. *J. Phys. Chem. A* **2012**, *116*, 1694-1700.
95. Geng, Y.; Takatani, T.; Hohenstein, E. G.; Sherrill, C. D., Accurately Characterizing the  $\Pi-\Pi$  Interaction Energies of Indole-Benzene Complexes. *J. Phys. Chem. A* **2010**, *114*, 3576-3582.
96. Braun, J.; Neusser, H. J.; Hobza, P., N-H $\cdots\Pi$  Interactions in Indole $\cdots$ Benzene-H<sub>6</sub>,D<sub>6</sub> and Indole $\cdots$ Benzene-H<sub>6</sub>,D<sub>6</sub> Radical Cation Complexes. Mass Analyzed Threshold Ionization Experiments and Correlated Ab Initio Quantum Chemical Calculations. *J. Phys. Chem. A* **2003**, *107*, 3918-3924.

97. Jurečka, P.; Šponer, J.; Černý, J.; Hobza, P., Benchmark Database of Accurate (Mp2 and Ccsd (T) Complete Basis Set Limit) Interaction Energies of Small Model Complexes, DNA Base Pairs, and Amino Acid Pairs. *Phys. Chem. Chem. Phys.* **2006**, *8*, 1985-1993.
98. Hobza, P.; Selzle, H. L.; Schlag, E. W., Potential Energy Surface of the Benzene Dimer: Ab Initio Theoretical Study. *J. Am. Chem. Soc.* **1994**, *116*, 3500-3506.
99. Wheeler, S. E.; Houk, K., Origin of Substituent Effects in Edge-to-Face Aryl–Aryl Interactions. *Mol. Phys.* **2009**, *107*, 749-760.
100. Lee, E. C.; Kim, D.; Jurecka, P.; Tarakeshwar, P.; Hobza, P.; Kim, K. S., Understanding of Assembly Phenomena by Aromatic–Aromatic Interactions: Benzene Dimer and the Substituted Systems. *J. Phys. Chem. A* **2007**, *111*, 3446-3457.
101. DiStasio Jr, R. A.; von Helden, G.; Steele, R. P.; Head-Gordon, M., On the T-Shaped Structures of the Benzene Dimer. *Chem. Phys. Lett.* **2007**, *437*, 277-283.
102. Pitonak, M.; Neogrady, P.; Rezac, J.; Jurecka, P.; Urban, M.; Hobza, P., Benzene Dimer: High-Level Wave Function and Density Functional Theory Calculations. *J. Chem. Theory. Comput.* **2008**, *4*, 1829-1834.
103. Frey, J. A.; Holzer, C.; Klopper, W.; Leutwyler, S., Experimental and Theoretical Determination of Dissociation Energies of Dispersion-Dominated Aromatic Molecular Complexes. *Chem. Rev.* **2016**, *116*, 5614-5641.
104. Ahnen, S.; Hehn, A.-S.; Vogiatzis, K. D.; Trachsel, M. A.; Leutwyler, S.; Klopper, W., Accurate Computations of the Structures and Binding Energies of the Imidazole... Benzene and Pyrrole... Benzene Complexes. *Chem. Phys.* **2014**, *441*, 17-22.
105. Ribas, J.; Cubero, E.; Luque, F. J.; Orozco, M., Theoretical Study of Alkyl- $\pi$  and Aryl- $\pi$  Interactions. Reconciling Theory and Experiment. *J. Org. Chem.* **2002**, *67*, 7057-7065.
106. Janowski, T.; Pulay, P., High Accuracy Benchmark Calculations on the Benzene Dimer Potential Energy Surface. *Chem. Phys. Lett.* **2007**, *447*, 27-32.
107. Duffy, E. M.; Kowalczyk, P. J.; Jorgensen, W. L., Do Denaturants Interact with Aromatic Hydrocarbons in Water? *J. Am. Chem. Soc.* **1993**, *115*, 9271-9275.
108. Soetens, J.-C.; Millot, C.; Chipot, C.; Jansen, G.; Ángyán, J. G.; Maigret, B., Effect of Polarizability on the Potential of Mean Force of Two Cations. The Guanidinium–Guanidinium Ion Pair in Water. *J. Phys. Chem. B* **1997**, *101*, 10910-10917.
109. Vazdar, M.; Uhlig, F.; Jungwirth, P., Like-Charge Ion Pairing in Water: An Ab Initio Molecular Dynamics Study of Aqueous Guanidinium Cations. *J. Phys. Chem. Lett.* **2012**, *3*, 2021-2024.
110. Vazdar, M.; Vymetal, J.; Heyda, J.; Vondrasek, J.; Jungwirth, P., Like-Charge Guanidinium Pairing from Molecular Dynamics and Ab Initio Calculations. *J. Phys. Chem. A* **2011**, *115*, 11193-11201.
111. Tesei, G.; Vazdar, M.; Jensen, M. R.; Cragnell, C.; Mason, P. E.; Heyda, J.; Skepö, M.; Jungwirth, P.; Lund, M., Self-Association of a Highly Charged Arginine-Rich Cell-Penetrating Peptide. *Proc. Natl. Acad. Sci. U. S. A.* **2017**, *114*, 11428-11433.
112. Inagaki, T.; Aono, S.; Nakano, H.; Yamamoto, T., Like-Charge Attraction of Molecular Cations in Water: Subtle Balance between Interionic Interactions and Ionic Solvation Effect. *J. Phys. Chem. B* **2014**, *118*, 5499-5508.
113. Maksimiak, K.; Rodziewicz-Motowidło, S.; Czaplewski, C.; Liwo, A.; Scheraga, H. A., Molecular Simulation Study of the Potentials of Mean Force for the Interactions between Models of Like-Charged and between Charged and Nonpolar Amino Acid Side Chains in Water. *J. Phys. Chem. B* **2003**, *107*, 13496-13504.
114. Shibasaki, K.; Fujii, A.; Mikami, N.; Tsuzuki, S., Magnitude of the Ch/ $\pi$  Interaction in the Gas Phase: Experimental and Theoretical Determination of the Accurate Interaction Energy in Benzene-Methane. *J. Phys. Chem. A* **2006**, *110*, 4397-4404.
115. Tsuzuki, S.; Honda, K.; Uchimaru, T.; Mikami, M.; Tanabe, K., The Magnitude of the Ch/ $\pi$  Interaction between Benzene and Some Model Hydrocarbons. *J. Am. Chem. Soc.* **2000**, *122*, 3746-3753.
116. Ringer, A. L.; Figgs, M. S.; Sinnokrot, M. O.; Sherrill, C. D., Aliphatic C–H/ $\pi$  Interactions: Methane–Benzene, Methane–Phenol, and Methane–Indole Complexes. *J. Phys. Chem. A* **2006**, *110*, 10822-10828.
117. Cao, Y.; Wong, M. W., Roles of Electrostatic Interaction and Dispersion in Ch... Ch, Ch...  $\pi$ , and  $\pi$ ...  $\pi$  Ethylene Dimers. *J. Mol. Model.* **2014**, *20*, 1-12.
118. Tsuzuki, S.; Lüthi, H. P., Interaction Energies of Van Der Waals and Hydrogen Bonded Systems Calculated Using Density Functional Theory: Assessing the Pw91 Model. *J. Chem. Phys.* **2001**, *114*, 3949-3957.
119. Kajander, T.; Kahn, P. C.; Passila, S. H.; Cohen, D. C.; Lehtio, L.; Adolfsen, W.; Warwicker, J.; Schell, U.; Goldman, A., Buried Charged Surface in Proteins. *Structure* **2000**, *8*, 1203-1214.
120. Ding, B.; Mukherjee, D.; Chen, J.; Gai, F., Do Guanidinium and Tetrapropylammonium Ions Specifically Interact with Aromatic Amino Acid Side Chains? *Proc. Natl. Acad. Sci. U. S. A.* **2017**, *114*, 1003-1008.
121. Mason, P. E.; Dempsey, C. E.; Neilson, G. W.; Kline, S. R.; Brady, J. W., Preferential Interactions of Guanidinium Ions with Aromatic Groups over Aliphatic Groups. *J. Am. Chem. Soc.* **2009**, *131*, 16689-16696.

122. König, G.; Boresch, S., Hydration Free Energies of Amino Acids: Why Side Chain Analog Data Are Not Enough. *J. Phys. Chem. B* **2009**, *113*, 8967-8974.
123. Roseman, M. A., Hydrophilicity of Polar Amino-Acid Side-Chains Is Markedly Reduced by Flanking Peptide-Bonds. *J. Mol. Biol.* **1988**, *200*, 513-522.
124. Wimley, W. C.; Creamer, T. P.; White, S. H., Solvation Energies of Amino Acid Side Chains and Backbone in a Family of Host-Guest Pentapeptides. *Biochemistry* **1996**, *35*, 5109-5124.
125. Yunger, L. M.; Cramer, R. D., 3rd, Measurement of Correlation of Partition Coefficients of Polar Amino Acids. *Mol. Pharmacol.* **1981**, *20*, 602-608.
126. Zheng, Y.-J.; Ornstein, R. L., What Happens to Salt-Bridges in Nonaqueous Environments: Insights from Quantum Mechanics Calculations. *J. Am. Chem. Soc.* **1996**, *118*, 11237-11243.
127. Nagy, P. I.; Erhardt, P. W., Theoretical Studies of Salt-Bridge Formation by Amino Acid Side Chains in Low and Medium Polarity Environments. *J. Phys. Chem. B* **2010**, *114*, 16436-16442.
128. Saigal, S.; Pranata, J., Monte Carlo Simulations of Guanidinium Acetate and Methylammonium Acetate Ion Pairs in Water. *Bioorg. Chem.* **1997**, *25*, 11-21.
129. Vener, M.; Odinkov, A.; Wehmeyer, C.; Sebastiani, D., The Structure and Ir Signatures of the Arginine-Glutamate Salt Bridge. Insights from the Classical Md Simulations. *J. Chem. Phys.* **2015**, *142*, 06B608\_601.
130. Sagarik, K.; Chaiyapongs, S., Structures and Stability of Salt-Bridge in Aqueous Solution. *Biophys. Chem.* **2005**, *117*, 119-140.
131. Shang, Y.; Nguyen, H.; Wickstrom, L.; Okur, A.; Simmerling, C., Improving the Description of Salt Bridge Strength and Geometry in a Generalized Born Model. *J. Mol. Graphics Modell.* **2011**, *29*, 676-684.
132. Hückel, E. Zur Theorie Der Elektrolyte. In *Ergebnisse Der Exakten Naturwissenschaften*; Springer: 1924, pp 199-276.
133. Parmar, A. S.; Muschol, M., Hydration and Hydrodynamic Interactions of Lysozyme: Effects of Chaotropic Versus Kosmotropic Ions. *Biophys. J.* **2009**, *97*, 590-598.
134. Neves, M. A.; Yeager, M.; Abagyan, R., Unusual Arginine Formations in Protein Function and Assembly: Rings, Strings, and Stacks. *J. Phys. Chem. B* **2012**, *116*, 7006-7013.
135. Vernon, R. M.; Chong, P. A.; Tsang, B.; Kim, T. H.; Bah, A.; Farber, P.; Lin, H.; Forman-Kay, J. D., Pi-Pi Contacts Are an Overlooked Protein Feature Relevant to Phase Separation. *eLife* **2018**, *7*, e31486.
136. Schmitt, C.; Bafna, J. A.; Schmid, B.; Klingl, S.; Baier, S.; Hemmis, B.; Wagner, R.; Winterhalter, M.; Voll, L. M., Manipulation of Charge Distribution in the Arginine and Glutamate Clusters of the Ompg Pore Alters Sugar Specificity and Ion Selectivity. *Biochim. Biophys. Acta, Biomembr.* **2019**, *1861*, 183021.
137. Pednekar, D.; Tendulkar, A.; Durani, S., Electrostatics-Defying Interaction between Arginine Termini as a Thermodynamic Driving Force in Protein-Protein Interaction. *Proteins* **2009**, *74*, 155-163.
138. Kroeger, T.; Frieg, B.; Zhang, T.; Hansen, F. K.; Marmann, A.; Proksch, P.; Nagel-Steger, L.; Groth, G.; Smits, S. H. J.; Gohlke, H., Edta Aggregates Induce Sypro Orange-Based Fluorescence in Thermal Shift Assay. *PLoS One* **2017**, *12*, e0177024.
139. Jacobson, A., Salt Effects on the Conformation of A-Poly-L-Glutamic Acid. *Biopolymers* **1964**, *2*, 237-244.
140. Jäger, C. M.; Hirsch, A.; Schade, B.; Ludwig, K.; Böttcher, C.; Clark, T., Self-Assembly of Structurally Persistent Micelles Is Controlled by Specific-Ion Effects and Hydrophobic Guests. *Langmuir* **2010**, *26*, 10460-10466.
141. Li, R.-Z.; Deng, S. H.; Hou, G.-L.; Valiev, M.; Wang, X.-B., Photoelectron Spectroscopy of Solvated Dicarboxylate and Alkali Metal Ion Clusters,  $M^+[O_2 C (CH_2)_2 Co_2]^{2-}[H_2 O] N$  ( $M = Na, K$ ;  $N = 1-6$ ). *Phys. Chem. Chem. Phys.* **2018**, *20*, 29051-29060.
142. Saenger, W., *Principles of Nucleic Acid Structure*. Springer Science and Business Media: 2013.
143. Muehldorf, A. V.; Van Engen, D.; Warner, J. C.; Hamilton, A. D., Aromatic-Aromatic Interactions in Molecular Recognition: A Family of Artificial Receptors for Thymine That Shows Both Face-to-Face and Edge-to-Face Orientations. *J. Am. Chem. Soc.* **1988**, *110*, 6561-6562.
144. Smithrud, D. B.; Diederich, F., Strength of Molecular Complexation of Apolar Solutes in Water and in Organic Solvents Is Predictable by Linear Free Energy Relationships: A General Model for Solvation Effects on Apolar Binding. *J. Am. Chem. Soc.* **1990**, *112*, 339-343.
145. Ferguson, S. B.; Sanford, E. M.; Seward, E. M.; Diederich, F., Cyclophane-Arene Inclusion Complexation in Protic Solvents: Solvent Effects Versus Electron Donor-Acceptor Interactions. *J. Am. Chem. Soc.* **1991**, *113*, 5410-5419.
146. Samanta, U.; Pal, D.; Chakrabarti, P., Packing of Aromatic Rings against Tryptophan Residues in Proteins. *Acta Crystallogr. Sect. D. Biol. Crystallogr.* **1999**, *55*, 1421-1427.
147. Singh, J.; Thornton, J., The Interaction between Phenylalanine Rings in Proteins. *FEBS Lett.* **1985**, *191*, 1-6.
148. Serrano, L.; Bycroft, M.; Fersht, A. R., Aromatic-Aromatic Interactions and Protein Stability: Investigation by Double-Mutant Cycles. *J. Mol. Biol.* **1991**, *218*, 465-475.
149. Hunter, C. A.; Singh, J.; Thornton, J. M.,  $\Pi$ - $\Pi$  Interactions: The Geometry and Energetics of Phenylalanine-Phenylalanine Interactions in Proteins. *J. Mol. Biol.* **1991**, *218*, 837-846.

150. McGaughey, G. B.; Gagné, M.; Rappé, A. K.,  $\Pi$ -Stacking Interactions: Alive and Well in Proteins\*. *J. Biol. Chem.* **1998**, *273*, 15458-15463.
151. Glyakina, A. V.; Bogatyreva, N. S.; Galzitskaya, O. V., Accessible Surfaces of Beta Proteins Increase with Increasing Protein Molecular Mass More Rapidly Than Those of Other Proteins. *PLoS One* **2011**, *6*, e28464.
152. Dyer, K., The Quiet Revolution: A New Synthesis of Biological Knowledge. *J. Biol. Educ.* **1971**, *5*, 15-24.
153. Hormoz, S., Amino Acid Composition of Proteins Reduces Deleterious Impact of Mutations. *Sci. Rep.* **2013**, *3*, 1-10.
154. Brooks, D. J.; Fresco, J. R.; Lesk, A. M.; Singh, M., Evolution of Amino Acid Frequencies in Proteins over Deep Time: Inferred Order of Introduction of Amino Acids into the Genetic Code. *Mol. Biol. Evol.* **2002**, *19*, 1645-1655.
155. Zhou, R., *Modeling of Nanotoxicity*. Springer: 2015.
156. Zorbas, V.; Smith, A. L.; Xie, H.; Ortiz-Acevedo, A.; Dalton, A. B.; Dieckmann, G. R.; Draper, R. K.; Baughman, R. H.; Musselman, I. H., Importance of Aromatic Content for Peptide/Single-Walled Carbon Nanotube Interactions. *J. Am. Chem. Soc.* **2005**, *127*, 12323-12328.
157. Wang, S.; Humphreys, E. S.; Chung, S.-Y.; Delduco, D. F.; Lustig, S. R.; Wang, H.; Parker, K. N.; Rizzo, N. W.; Subramoney, S.; Chiang, Y.-M., Peptides with Selective Affinity for Carbon Nanotubes. *Nat. Mater.* **2003**, *2*, 196-200.
158. Ge, C.; Du, J.; Zhao, L.; Wang, L.; Liu, Y.; Li, D.; Yang, Y.; Zhou, R.; Zhao, Y.; Chai, Z., Binding of Blood Proteins to Carbon Nanotubes Reduces Cytotoxicity. *Proc. Natl. Acad. Sci. U. S. A.* **2011**, *108*, 16968-16973.
159. Tachikawa, H.; Miyazawa, Y.; Iura, R., Timescale of  $\Pi$ -Stacking Formation in a Benzene Trimer Cation Formed by Ionization of the Parent Neutral Trimer: A Direct Ab Initio Molecular Dynamics Study. *ChemistrySelect* **2018**, *3*, 1113-1119.
160. Mason, P.; Dempsey, C.; Neilson, G.; Brady, J., Nanometer-Scale Ion Aggregates in Aqueous Electrolyte Solutions: Guanidinium Sulfate and Guanidinium Thiocyanate. *J. Phys. Chem. B* **2005**, *109*, 24185-24196.
161. Li, S.; Hong, M., Protonation, Tautomerization, and Rotameric Structure of Histidine: A Comprehensive Study by Magic-Angle-Spinning Solid-State Nmr. *J. Am. Chem. Soc.* **2011**, *133*, 1534-1544.
162. Sharma, V.; Wang, Y.-S.; Liu, W. R., Probing the Catalytic Charge-Relay System in Alanine Racemase with Genetically Encoded Histidine Mimetics. *ACS Chem. Biol.* **2016**, *11*, 3305-3309.
163. Krishna Deepak, R. N. V.; Sankaramakrishnan, R., N-H $\cdots$ N Hydrogen Bonds Involving Histidine Imidazole Nitrogen Atoms: A New Structural Role for Histidine Residues in Proteins. *Biochemistry* **2016**, *55*, 3774-3783.
164. McGaughey, G. B.; Gagné, M.; Rappé, A. K.,  $\Pi$ -Stacking Interactions: Alive and Well in Proteins. *J. Biol. Chem.* **1998**, *273*, 15458-15463.
165. Liao, S. M.; Du, Q. S.; Meng, J. Z.; Pang, Z. W.; Huang, R. B., The Multiple Roles of Histidine in Protein Interactions. *Chem. Cent. J.* **2013**, *7*, 44.
166. Rauwerdink, A.; Kazlauskas, R. J., How the Same Core Catalytic Machinery Catalyzes 17 Different Reactions: The Serine-Histidine-Aspartate Catalytic Triad of A/B-Hydrolase Fold Enzymes. *ACS Catal.* **2015**, *5*, 6153-6176.
167. Mei, B.; Zalkin, H., A Cysteine-Histidine-Aspartate Catalytic Triad Is Involved in Glutamine Amide Transfer Function in Purf-Type Glutamine Amidotransferases. *J. Biol. Chem.* **1989**, *264*, 16613-16619.
168. Van Pouderoyen, G.; Eggert, T.; Jaeger, K.-E.; Dijkstra, B. W., The Crystal Structure of Bacillus Subtilis Lipase: A Minimal A/B Hydrolase Fold Enzyme. *J. Mol. Biol.* **2001**, *309*, 215-226.
169. Uppula, P., Exploration of Conformations, Analysis of Protein and Biological Significance of Histidine Dimers. *ChemistrySelect* **2018**, *3*, 3070-3078.
170. Matthews, R. P.; Welton, T.; Hunt, P. A., Hydrogen Bonding and  $\Pi$ - $\Pi$  Interactions in Imidazolium-Chloride Ionic Liquid Clusters. *Phys. Chem. Chem. Phys.* **2015**, *17*, 14437-14453.
171. Kar, P.; Biswas, R.; Drew, M. G. B.; Frontera, A.; Ghosh, A., Host-Guest Supramolecular Interactions in the Coordination Compounds of 4,4'-Azobis(Pyridine) with Mnx2 (X = Ncs-, Ncn-, and Pf6-): Structural Analyses and Theoretical Study. *Inorg. Chem.* **2012**, *51*, 1837-1851.
172. Churchill, C. D.; Wetmore, S. D., Noncovalent Interactions Involving Histidine: The Effect of Charge on  $\Pi$ - $\Pi$  Stacking and T-Shaped Interactions with the DNA Nucleobases. *J. Phys. Chem. B* **2009**, *113*, 16046-16058.
173. Grover, J.; Walters, E.; Hui, E., Dissociation Energies of the Benzene Dimer and Dimer Cation. *J. Phys. Chem.* **1987**, *91*, 3233-3237.
174. Scrutton, N. S.; Raine, A. R., Cation- $\Pi$  Bonding and Amino-Aromatic Interactions in the Biomolecular Recognition of Substituted Ammonium Ligands. *Biochem. J.* **1996**, *319*, 1-8.
175. Burley, S.; Petsko, G., Amino-Aromatic Interactions in Proteins. *FEBS Lett.* **1986**, *203*, 139-143.
176. Dougherty, D. A., Cation- $\Pi$  Interactions in Chemistry and Biology: A New View of Benzene, Phe, Tyr, and Trp. *Science* **1996**, *271*, 163-168.

177. Kumar, K.; Woo, S. M.; Siu, T.; Cortopassi, W. A.; Duarte, F.; Paton, R. S., Cation– $\Pi$  Interactions in Protein–Ligand Binding: Theory and Data-Mining Reveal Different Roles for Lysine and Arginine. *Chem. Sci.* **2018**, *9*, 2655-2665.
178. Singh, N. J.; Min, S. K.; Kim, D. Y.; Kim, K. S., Comprehensive Energy Analysis for Various Types of  $\Pi$ -Interaction. *J. Chem. Theory. Comput.* **2009**, *5*, 515-529.
179. Kubíčková, A.; Křížek, T. s.; Coufal, P.; Wernersson, E.; Heyda, J.; Jungwirth, P., Guanidinium Cations Pair with Positively Charged Arginine Side Chains in Water. *J. Phys. Chem. Lett.* **2011**, *2*, 1387-1389.
180. Shih, O.; England, A. H.; Dallinger, G. C.; Smith, J. W.; Duffey, K. C.; Cohen, R. C.; Prendergast, D.; Saykally, R. J., Cation-Cation Contact Pairing in Water: Guanidinium. *J. Chem. Phys.* **2013**, *139*, 035104.
181. Biswas, B.; Singh, P. C., The Unusual Visible Fluorescence Violating the Kasha's Rule Suggests the Aggregation of Guanidinium Carbonate in Its Aqueous Medium. *J. Mol. Liq.* **2018**, *253*, 211-216.
182. Marsili, S.; Chelli, R.; Schettino, V.; Procacci, P., Thermodynamics of Stacking Interactions in Proteins. *Phys. Chem. Chem. Phys.* **2008**, *10*, 2673-2685.
183. Vondrášek, J. í.; Mason, P. E.; Heyda, J.; Collins, K. D.; Jungwirth, P., The Molecular Origin of Like-Charge Arginine–Arginine Pairing in Water. *J. Phys. Chem. B* **2009**, *113*, 9041-9045.
184. Lee, D.; Lee, J.; Seok, C., What Stabilizes Close Arginine Pairing in Proteins? *Phys. Chem. Chem. Phys.* **2013**, *15*, 5844-5853.
185. Mason, P. E.; Neilson, G. W.; Enderby, J. E.; Sabounji, M.-L.; Dempsey, C. E.; MacKerell Jr, A. D.; Brady, J. W., The Structure of Aqueous Guanidinium Chloride Solutions. *J. Am. Chem. Soc.* **2004**, *126*, 11462-11470.
186. Maier, J. A.; Martinez, C.; Kasavajhala, K.; Wickstrom, L.; Hauser, K. E.; Simmerling, C., Ff14sb: Improving the Accuracy of Protein Side Chain and Backbone Parameters from Ff99sb. *Journal of Chemical Theory and Computation* **2015**, *11*, 3696-3713.
187. Wang, J.; Wolf, R. M.; Caldwell, J. W.; Kollman, P. A.; Case, D. A., Development and Testing of a General Amber Force Field. *J. Comput. Chem.* **2004**, *25*, 1157-1174.
188. Izadi, S.; Anandakrishnan, R.; Onufriev, A. V., Building Water Models: A Different Approach. *J. Phys. Chem. Lett.* **2014**, *5*, 3863-3871.
189. Bayly, C. I.; Cieplak, P.; Cornell, W. D.; Kollman, P. A., A Well-Behaved Electrostatic Potential Based Method Using Charge Restraints for Deriving Atomic Charges - the Resp Model. *J. Phys. Chem.* **1993**, *97*, 10269-10280.
190. Sprenger, K. G.; Jaeger, V. W.; Pfaendtner, J., The General Amber Force Field (Gaff) Can Accurately Predict Thermodynamic and Transport Properties of Many Ionic Liquids. *J. Phys. Chem. B* **2015**, *119*, 5882-5895.
191. Johnson, M. E.; Malardier-Jugroot, C.; Murarka, R. K.; Head-Gordon, T., Hydration Water Dynamics near Biological Interfaces. *J. Phys. Chem. B* **2009**, *113*, 4082-4092.
192. Nerenberg, P. S.; Jo, B.; So, C.; Tripathy, A.; Head-Gordon, T., Optimizing Solute–Water Van Der Waals Interactions to Reproduce Solvation Free Energies. *J. Phys. Chem. B* **2012**, *116*, 4524-4534.
193. Lay, W. K.; Miller, M. S.; Elcock, A. H., Reparameterization of Solute-Solute Interactions for Amino Acid-Sugar Systems Using Isopiestic Osmotic Pressure Molecular Dynamics Simulations. *J. Chem. Theory. Comput.* **2017**, *13*, 1874-1882.
194. Yoo, J.; Aksimentiev, A., New Tricks for Old Dogs: Improving the Accuracy of Biomolecular Force Fields by Pair-Specific Corrections to Non-Bonded Interactions. *Phys. Chem. Chem. Phys.* **2018**, *20*, 8432-8449.
195. Bedrov, D.; Piquemal, J. P.; Borodin, O.; MacKerell, A. D.; Roux, B.; Schroder, C., Molecular Dynamics Simulations of Ionic Liquids and Electrolytes Using Polarizable Force Fields. *Chem. Rev.* **2019**, *119*, 7940-7995.
196. Yoo, J.; Aksimentiev, A., Improved Parameterization of Amine–Carboxylate and Amine–Phosphate Interactions for Molecular Dynamics Simulations Using the Charmm and Amber Force Fields. *J. Chem. Theory. Comput.* **2016**, *12*, 430-443.
197. Leontyev, I.; Stuchebrukhov, A., Accounting for Electronic Polarization in Non-Polarizable Force Fields. *Phys. Chem. Chem. Phys.* **2011**, *13*, 2613-2626.
198. Yoo, J.; Aksimentiev, A., Refined Parameterization of Nonbonded Interactions Improves Conformational Sampling and Kinetics of Protein Folding Simulations. *J. Phys. Chem. Lett.* **2016**, *7*, 3812-3818.
199. Yoo, J.; Wilson, J.; Aksimentiev, A., Improved Model of Hydrated Calcium Ion for Molecular Dynamics Simulations Using Classical Biomolecular Force Fields. *Biopolymers* **2016**, *105*, 752-763.
200. Miller, M. S.; Lay, W. K.; Elcock, A. H., Osmotic Pressure Simulations of Amino Acids and Peptides Highlight Potential Routes to Protein Force Field Parameterization. *J. Phys. Chem. B* **2016**, *120*, 8217-8229.
201. Miller, M. S.; Lay, W. K.; Li, S.; Hacker, W. C.; An, J.; Ren, J.; Elcock, A. H., Reparametrization of Protein Force Field Nonbonded Interactions Guided by Osmotic Coefficient Measurements from Molecular Dynamics Simulations. *J. Chem. Theory. Comput.* **2017**, *13*, 1812-1826.
202. Berneche, S.; Roux, B., Energetics of Ion Conduction through the K<sup>+</sup> Channel. *Nature* **2001**, *414*, 73-77.
203. Luo, Y.; Roux, B., Simulation of Osmotic Pressure in Concentrated Aqueous Salt Solutions. *J. Phys. Chem. Lett.* **2010**, *1*, 183-189.

204. Lukasheva, N.; Tolmachev, D.; Martinez-Seara, H.; Karttunen, M., Changes in the Local Conformational States Caused by Simple Na<sup>+</sup> and K<sup>+</sup> Ions in Polyelectrolyte Simulations: Comparison of Seven Force Fields with and without Nbfix and Ecc Corrections. *Polymers* **2022**, *14*, 252.
205. Honig, B.; Sharp, K.; Yang, A. S., Macroscopic Models of Aqueous Solutions: Biological and Chemical Applications. *J. Phys. Chem.* **1993**, *97*, 1101-1109.
206. Still, W. C.; Tempczyk, A.; Hawley, R. C.; Hendrickson, T., Semianalytical Treatment of Solvation for Molecular Mechanics and Dynamics. *J. Am. Chem. Soc.* **1990**, *112*, 6127-6129.
207. Dominy, B. N.; Brooks, C. L., Development of a Generalized Born Model Parametrization for Proteins and Nucleic Acids. *J. Phys. Chem. B* **1999**, *103*, 3765-3773.
208. Lazaridis, T.; Karplus, M., Effective Energy Function for Proteins in Solution. *Proteins* **1999**, *35*, 133-152.
209. Swanson, J. M.; Mongan, J.; McCammon, J. A., Limitations of Atom-Centered Dielectric Functions in Implicit Solvent Models. *J. Phys. Chem. B* **2005**, *109*, 14769-14772.
210. Hendsch, Z. S.; Tidor, B., Do Salt Bridges Stabilize Proteins? A Continuum Electrostatic Analysis. *Protein Sci.* **1994**, *3*, 211-226.
211. Mongan, J.; Simmerling, C.; McCammon, J. A.; Case, D. A.; Onufriev, A., Generalized Born Model with a Simple, Robust Molecular Volume Correction. *J. Chem. Theory. Comput.* **2007**, *3*, 156-169.
212. Colla, T.; Nunes Lopes, L.; Dos Santos, A. P., Ionic Size Effects on the Poisson-Boltzmann Theory. *J. Chem. Phys.* **2017**, *147*, 014104.
213. Pitera, J. W.; Swope, W., Understanding Folding and Design: Replica-Exchange Simulations of "Trp-Cage" Miniproteins. *Proc. Natl. Acad. Sci. U. S. A.* **2003**, *100*, 7587-7592.
214. Felts, A. K.; Harano, Y.; Gallicchio, E.; Levy, R. M., Free Energy Surfaces of B-Hairpin and A-Helical Peptides Generated by Replica Exchange Molecular Dynamics with the Agbnp Implicit Solvent Model. *Proteins* **2004**, *56*, 310-321.
215. Zhou, R., Free Energy Landscape of Protein Folding in Water: Explicit Vs. Implicit Solvent. *Proteins* **2003**, *53*, 148-161.
216. Zhou, R.; Berne, B. J., Can a Continuum Solvent Model Reproduce the Free Energy Landscape of a B-Hairpin Folding in Water? *Proc. Natl. Acad. Sci. U. S. A.* **2002**, *99*, 12777-12782.
217. Woo, H. J.; Roux, B., Calculation of Absolute Protein-Ligand Binding Free Energy from Computer Simulations. *Proc. Natl. Acad. Sci. U. S. A.* **2005**, *102*, 6825-6830.
218. Helms, V.; Wade, R. C., Computational Alchemy to Calculate Absolute Protein-Ligand Binding Free Energy. *J. Am. Chem. Soc.* **1998**, *120*, 2710-2713.
219. Hermans, J.; Shankar, S., The Free-Energy of Xenon Binding to Myoglobin from Molecular-Dynamics Simulation. *Isr. J. Chem.* **1986**, *27*, 225-227.
220. Roux, B.; Nina, M.; Pomes, R.; Smith, J. C., Thermodynamic Stability of Water Molecules in the Bacteriorhodopsin Proton Channel: A Molecular Dynamics Free Energy Perturbation Study. *Biophys. J.* **1996**, *71*, 670-681.
221. Dzubiella, J., Salt-Specific Stability and Denaturation of a Short Salt-Bridge-Forming A-Helix. *J. Am. Chem. Soc.* **2008**, *130*, 14000-14007.
222. Weber, D. S.; Warren, J. J., The Interaction between Methionine and Two Aromatic Amino Acids Is an Abundant and Multifunctional Motif in Proteins. *Arch. Biochem. Biophys.* **2019**, *672*, 108053.
223. Fedorov, M. V.; Goodman, J. M.; Schumm, S., The Effect of Sodium Chloride on Poly-L-Glutamate Conformation. *Chem. Commun.* **2009**, 896-898.
224. Mazzini, V.; Craig, V. S., Volcano Plots Emerge from a Sea of Nonaqueous Solvents: The Law of Matching Water Affinities Extends to All Solvents. *ACS Cent. Sci.* **2018**, *4*, 1056-1064.
225. Collins, K. D., Charge Density-Dependent Strength of Hydration and Biological Structure. *Biophys. J.* **1997**, *72*, 65-76.
226. Hess, B.; van der Vegt, N. F., Cation Specific Binding with Protein Surface Charges. *Proc. Natl. Acad. Sci. U. S. A.* **2009**, *106*, 13296-13300.
227. Vrbka, L.; Vondrášek, J.; Jagoda-Cwiklik, B.; Vácha, R.; Jungwirth, P., Quantification and Rationalization of the Higher Affinity of Sodium over Potassium to Protein Surfaces. *Proc. Natl. Acad. Sci. U. S. A.* **2006**, *103*, 15440-15444.
228. Chandler, D., Interfaces and the Driving Force of Hydrophobic Assembly. *Nature* **2005**, *437*, 640-647.
229. Southall, N. T.; Dill, K. A., The Mechanism of Hydrophobic Solvation Depends on Solute Radius. *J. Phys. Chem. B* **2000**, *104*, 1326-1331.
230. Heyda, J.; Vincent, J. C.; Tobias, D. J.; Dzubiella, J.; Jungwirth, P., Ion Specificity at the Peptide Bond: Molecular Dynamics Simulations of N-Methylacetamide in Aqueous Salt Solutions. *J. Phys. Chem. B* **2010**, *114*, 1213-1220.

231. Sukenik, S.; Boyarski, Y.; Harries, D., Effect of Salt on the Formation of Salt-Bridges in B-Hairpin Peptides. *Chem. Commun.* **2014**, *50*, 8193-8196.
232. Zhao, H., Effect of Ions and Other Compatible Solutes on Enzyme Activity, and Its Implication for Biocatalysis Using Ionic Liquids. *J. Mol. Catal. B: Enzym.* **2005**, *37*, 16-25.
233. Zhao, H., Are Ionic Liquids Kosmotropic or Chaotropic? An Evaluation of Available Thermodynamic Parameters for Quantifying the Ion Kosmotropicity of Ionic Liquids. *J. Chem. Technol. Biotechnol.* **2006**, *81*, 877-891.
234. Kumar, A.; Rani, A.; Venkatesu, P., A Comparative Study of the Effects of the Hofmeister Series Anions of the Ionic Salts and Ionic Liquids on the Stability of A-Chymotrypsin. *New J. Chem.* **2015**, *39*, 938-952.
235. Lei, Z.; Chen, B.; Koo, Y.-M.; MacFarlane, D. R., Introduction: Ionic Liquids. **2017**, *117*, 6633-6635.
236. Kokh, D. B.; Doser, B.; Richter, S.; Ormersbach, F.; Cheng, X.; Wade, R. C., A Workflow for Exploring Ligand Dissociation from a Macromolecule: Efficient Random Acceleration Molecular Dynamics Simulation and Interaction Fingerprint Analysis of Ligand Trajectories. *J. Chem. Phys.* **2020**, *153*, 125102.
237. Martinez, L.; Andrade, R.; Birgin, E. G.; Martinez, J. M., Packmol: A Package for Building Initial Configurations for Molecular Dynamics Simulations. *J. Comput. Chem.* **2009**, *30*, 2157-2164.
238. Schott-Verdugo, S.; Gohlke, H., Packmol-Memgen: A Simple-to-Use, Generalized Workflow for Membrane-Protein-Lipid-Bilayer System Building. *J. Chem. Inf. Model.* **2019**, *59*, 2522-2528.
239. Word, J. M.; Lovell, S. C.; Richardson, J. S.; Richardson, D. C., Asparagine and Glutamine: Using Hydrogen Atom Contacts in the Choice of Side-Chain Amide Orientation. *J. Mol. Biol.* **1999**, *285*, 1735-1747.
240. Schafmeister, C. E. A. F.; Ross, W. S.; Romanovski, V. *Leap*, University of California, San Francisco, 1995.
241. Case, D. A.; Ben-Shalom, I. Y.; Brozell, S. R.; Cerutti, D. S.; Cheatham III, T. E. V. W. D.; Darden, T. A.; Duke, R. E.; Ghoreishi, D.; Gilson, M. K.; Gohlke, H.; Goetz, A. W.; Greene, D.; Harris, R.; Homeyer, N.; Izadi, S.; Kovalenko, A.; Kurtzman, T.; Lee, T. S.; LeGrand, S.; Li, P.; Lin, C.; Liu, J.; Luchko, T.; Luo, R.; Mermelstein, D. J.; Merz, K. M.; Miao, Y.; Monard, G.; Nguyen, C.; Nguyen, H.; Omelyan, I.; Onufriev, A.; Pan, F.; Qi, R.; Roe, D. R.; Roitberg, A.; Sagui, C.; Schott-Verdugo, S.; Shen, J.; Simmerling, C. L.; Smith, J.; Salomon-Ferrer, R.; Swails, J.; Walker, R. C.; Wang, J.; Wei, H.; Wolf, R. M.; Wu, X.; Xiao, L.; York, D. M.; Kollman, P. A. *Amber 2018*, University of California, San Francisco, 2018.
242. Frisch, M. J.; Trucks, G. W.; Schlegel, H. B.; Scuseria, G. E.; Robb, M. A.; Cheeseman, J. R.; Scalmani, G.; Barone, V.; Petersson, G. A.; Nakatsuji, H.; Li, X.; Caricato, M.; Marenich, A. V.; Bloino, J.; Janesko, B. G.; Gomperts, R.; Mennucci, B.; Hratchian, H. P.; Ortiz, J. V.; Izmaylov, A. F.; Sonnenberg, J. L.; Williams; Ding, F.; Lipparini, F.; Egidi, F.; Goings, J.; Peng, B.; Petrone, A.; Henderson, T.; Ranasinghe, D.; Zakrzewski, V. G.; Gao, J.; Rega, N.; Zheng, G.; Liang, W.; Hada, M.; Ehara, M.; Toyota, K.; Fukuda, R.; Hasegawa, J.; Ishida, M.; Nakajima, T.; Honda, Y.; Kitao, O.; Nakai, H.; Vreven, T.; Throssell, K.; Montgomery Jr., J. A.; Peralta, J. E.; Ogliaro, F.; Bearpark, M. J.; Heyd, J. J.; Brothers, E. N.; Kudin, K. N.; Staroverov, V. N.; Keith, T. A.; Kobayashi, R.; Normand, J.; Raghavachari, K.; Rendell, A. P.; Burant, J. C.; Iyengar, S. S.; Tomasi, J.; Cossi, M.; Millam, J. M.; Klene, M.; Adamo, C.; Cammi, R.; Ochterski, J. W.; Martin, R. L.; Morokuma, K.; Farkas, O.; Foresman, J. B.; Fox, D. J. *Gaussian 16 Rev. A.03*, Wallingford, CT, 2016.
243. Roothaan, C. C. J., New Developments in Molecular Orbital Theory. *Rev. Mod. Phys.* **1951**, *23*, 69-89.
244. Friege, B.; Gorg, B.; Homeyer, N.; Keitel, V.; Haussinger, D.; Gohlke, H., Molecular Mechanisms of Glutamine Synthetase Mutations That Lead to Clinically Relevant Pathologies. *PLoS Comput. Biol.* **2016**, *12*, e1004693.
245. Darden, T.; York, D.; Pedersen, L., Particle Mesh Ewald - an N.Log(N) Method for Ewald Sums in Large Systems. *J. Chem. Phys.* **1993**, *98*, 10089-10092.
246. Berendsen, H. J.; Postma, J. v.; Van Gunsteren, W. F.; DiNola, A.; Haak, J. R., Molecular Dynamics with Coupling to an External Bath. *J. Chem. Phys.* **1984**, *81*, 3684-3690.
247. Ryckaert, J.-P.; Ciccotti, G.; Berendsen, H. J. C., Numerical Integration of the Cartesian Equations of Motion of a System with Constraints: Molecular Dynamics of N-Alkanes. *J. Comput. Phys.* **1977**, *23*, 327-341.
248. Hopkins, C. W.; Le Grand, S.; Walker, R. C.; Roitberg, A. E., Long-Time-Step Molecular Dynamics through Hydrogen Mass Repartitioning. *J. Chem. Theory. Comput.* **2015**, *11*, 1864-1874.
249. Grossfield, A. *Wham: The Weighted Histogram Analysis Method*, Version 2.0.7, [http://membrane.urmc.rochester.edu/wordpress/?page\\_id=126](http://membrane.urmc.rochester.edu/wordpress/?page_id=126).
250. Roe, D. R.; Cheatham, T. E., 3rd, Ptraj and Cpptraj: Software for Processing and Analysis of Molecular Dynamics Trajectory Data. *J. Chem. Theory. Comput.* **2013**, *9*, 3084-3095.



## 12 Table of Contents Graphic

